

## Sediment archives reveal irreversible shifts in plankton communities after World War II and agricultural pollution

Siano Raffaele <sup>1,\*</sup>, Lassudrie Duchesne Malwenn <sup>2</sup>, Cuzin Pierre <sup>3</sup>, Briant Nicolas <sup>4</sup>, Loizeau Veronique <sup>5</sup>, Schmidt Sabine <sup>6</sup>, Ehrhold Axel <sup>7</sup>, Mertens Kenneth <sup>2</sup>, Lambert Clément <sup>8</sup>, Quintric Laure <sup>3</sup>, Noël Cyril <sup>3</sup>, Latimier Marie <sup>1</sup>, Quéré Julien <sup>1</sup>, Durand Patrick <sup>3</sup>, Penaud Aurélie <sup>9</sup>

<sup>1</sup> Ifremer, DYNECO, 29280 Plouzané, France

<sup>2</sup> Ifremer, LITTORAL LER BO, Station de Biologie Marine, Place de la Croix, BP40537, 29900 Concarneau Cedex, France

<sup>3</sup> Ifremer, SeBiMER, 29280 Plouzané, France

<sup>4</sup> Ifremer, BE, 44311 Nantes, France

<sup>5</sup> Ifremer, PFOM, 29280 Plouzané, France

<sup>6</sup> CNRS, UMR 5805 EPOC, Université de Bordeaux, Pessac, France

<sup>7</sup> Ifremer, GM, 29280 Plouzané, France

<sup>8</sup> UMR 6538 Laboratoire Géosciences Océan (LGO), Université de Bretagne Sud (UBS), 56000 Vannes, France

<sup>9</sup> CNRS, UMR 6538 Laboratoire Géosciences Océan (LGO), Université de Brest (UBO), 29280 Plouzané, France

\* Corresponding author : Raffaele Siano, email address : [raffaele.siano@ifremer.fr](mailto:raffaele.siano@ifremer.fr)

### Abstract :

To evaluate the stability and resilience<sup>1</sup> of coastal ecosystem communities to perturbations that occurred during the Anthropocene,<sup>2</sup> pre-industrial biodiversity baselines inferred from paleoarchives are needed.<sup>3,4</sup> The study of ancient DNA (aDNA) from sediments (sedaDNA)<sup>5</sup> has provided valuable information about past dynamics of microbial species<sup>6, 7, 8</sup> and communities<sup>9, 10, 11, 12, 13, 14, 15, 16, 17, 18</sup> in relation to ecosystem variations. Shifts in planktonic protist communities might significantly affect marine ecosystems through cascading effects,<sup>19, 20, 21</sup> and therefore the analysis of this compartment is essential for the assessment of ecosystem variations. Here, sediment cores collected from different sites of the Bay of Brest (northeast Atlantic, France) allowed ca. 1,400 years of retrospective analyses of the effects of human pollution on marine protists. Comparison of sedaDNA extractions and metabarcoding analyses with different barcode regions (V4 and V7 18S rDNA) revealed that protist assemblages in ancient sediments are mainly composed of species known to produce resting stages. Heavy-metal pollution traces in sediments were ascribed to the World War II period and coincided with community shifts within dinoflagellates and stramenopiles. After the war and especially from the 1980s to 1990s, protist genera shifts followed chronic contaminations of agricultural origin. Community composition reconstruction over time showed that there was no recovery to a Middle Ages baseline composition. This demonstrates the irreversibility of the observed shifts after the cumulative effect of war and agricultural pollutions. Developing a paleoecological approach, this study highlights how human contaminations

---

irreversibly affect marine microbial compartments, which contributes to the debate on coastal ecosystem preservation and restoration.

47 **Results and Discussion**

48 **Paleocommunity diversity of marine coastal ecosystems**

49 Biological analyses on microeukaryotic (protist) communities were inferred from sediment cores  
50 collected at three different sites of the Bay of Brest (Figure S1A) covering about 72 (Elorn Estuary  
51 core [EE] Data S1A), 99 (Daoulas Estuary core [DE] Data S1B) and 5000 calendar years (cal. yr.)  
52 (Brest Harbor core (BH), Figure S1B, Data S1C, Video S1). The multiple sedimentary ancient DNA  
53 (*sedaDNA*) extraction methods combined with a double metabarcoding analysis that were applied  
54 to the BH core provided new information for the future establishment of a general protocol for  
55 marine *sedaDNA* studies. After validation on the BH core, this approach was applied to EE and DE  
56 cores. By comparing total (TOT), intracellular (IN) and extracellular (EX) *sedaDNA* extraction  
57 methods (Table S1, Figure S2A, Figure S2B), and the  $\alpha$  and  $\beta$  protist diversities obtained from two  
58 different barcode sizes (V4 [ca. 390 bp, base pairs] and V7 [ca. 200 bp] of the 18S ribosomal DNA  
59 [rDNA] gene region) (Table S2), it was found that the total *sedaDNA* extraction method allowed  
60 the analysis of mostly intracellular DNA (Figure S2C, Figure S2D). Over the entire BH core, up to  
61 69% of V7 and 58% of V4 Amplicon Sequence Variants (ASVs) that were  $\geq 1\%$  abundant in the  
62 TOT extracts, were also present in the IN fraction (Figure S2E). Our study confirms Armbrrecht et  
63 al.'s<sup>22</sup> hypothesis that extraction techniques targeting only extracellular DNA, as those used in  
64 terrestrial ecological surveys<sup>23,24</sup>, are not suitable for marine *sedaDNA* studies of protists. Given  
65 the ability of many protists to form benthic, sedimentary resting stages that protect cellular  
66 content—including the nucleus—it is considered that the retrieved intracellular protist DNA is  
67 extracted from resting stages. Indeed, 83% (V7) and 82% (V4) of the common ASVs were assigned  
68 to protist genera known to include species that can produce resting stages (Data S2). It is suggested  
69 that the amplification of total *sedaDNA* allows diversity analyses of mostly protist resting stages  
70 and that eukaryotic DNA archives in ancient sediments mostly correspond to assemblages of protist  
71 resting stages, that are defined here as paleocommunities.

72 BH sediment samples could be separated into two groups according to ASV richness and  $\beta$   
73 diversities (Figure S2D). This difference was attributed *sedaDNA* preservation issues in sandy

74 lower deposits of deeper core layers. Therefore, only the first upper section of the BH core (0-231  
75 cm, ca. 1400 years from the Middle Ages [V<sup>th</sup>–VI<sup>th</sup> centuries] to the contemporary era [XXI<sup>th</sup>  
76 century]) was considered for biodiversity analyses (Figure S2F). *SedaDNA* metabarcoding analyses  
77 of the BH core showed that the long (V4) and the shorter (V7) fragments provided a similar  
78 diversity for eukaryotic paleocommunities (Figure 1). Although only some eukaryotic groups were  
79 identified by V7 metabarcoding (unknown Archaeplastida, Telonemia), V4 analysis allowed to  
80 identify more groups than V7 (33 vs 27). Therefore, only V4 was considered in the subsequent  
81 ecological analyses of the Bay of Brest cores. Degradation of *sedaDNA* involves DNA  
82 fragmentation<sup>22</sup>, therefore the length of the barcode used in metabarcoding influences biodiversity  
83 analyses. The amplification of ca. 500 bp fragments from ancient sediment for some protist species  
84 was previously reported in ancient sediments (e.g.<sup>10</sup>). In agreement with previous results, here it is  
85 demonstrated that ca. 400 bp DNA fragment analyses are also suitable for assessing the diversity  
86 of a large fraction of the protist community, confirming that the previous validation of the V4  
87 approach of Medieval (until ca. AD 900) to modern sediment from freshwater environments<sup>13</sup> also  
88 works for coastal marine ecosystems.

89 Paleocommunities of the BH core were mostly composed of three divisions: Alveolata,  
90 Opisthokonta, and Archaeplastida, dominated respectively by Apicomplexa (average: 33%),  
91 Metazoa (12%), and Streptophyta (8%). Dinoflagellata (Alveolata) (6%) were the fourth abundant  
92 group. Unassigned eukaryotic ASV (Unknown) accounted for on average 28% of the  
93 paleocommunity biodiversity (Figure 1, right panel). The relative importance of the most important  
94 groups varied throughout the core. Metazoa largely dominated in superficial sediments (3–11 cm;  
95 average: 45%, max: 70%) with Annelida ASV as the most representative phylum (average 38%).  
96 The protist group of Apicomplexa usually dominated throughout the rest of the BH core (13–231  
97 cm; average: 30%; max: 59%; Figure 1) and the EE and DE cores (Figure S3). Within this group  
98 the invertebrate parasitic class of gregarines were prevalent (average: 25%; max: 55% of total

99 eukaryotes), dominated by three genera of invertebrate coelomic parasites<sup>25</sup> (average, max:  
100 *Lecudina*, 15%, 50%; *Lankesteria*, 2%, 8%; *Selenidium*, 1%, 8%). Dinoflagellates were  
101 occasionally abundant both in superficial (22%; 23%) and in deeper sediments (14%; 20%).

102 Paleocommunities differ from both superficial sediment and planktonic protist  
103 communities. In plankton communities, the supergroup of Alveolata (specifically Marine  
104 ALVeolates (MALVs) and dinoflagellates) dominate together with Rhizaria and Stramenopiles  
105 (particularly Bacillariophyta), respectively, the offshore<sup>26</sup> and the coastal protist communities<sup>27</sup>.  
106 Superficial sediment communities are dominated by Rhizaria (in particular Cercozoa), Alveolata  
107 (Ciliophora), and Stramenopiles (Bacillariophyta), and share < 10% of the species richness with the  
108 planktonic community<sup>28</sup>. The dominance or high proportion of gregarines, a resting-stage-forming  
109 group of metazoan parasites<sup>29</sup>, can be considered a specific protist biodiversity pattern of marine  
110 sediment archives. Indeed, Apicomplexa were also found abundant in marine sedimentary archives  
111 of the Arabian Sea and associated to depleted oxygen conditions<sup>15</sup>. Gregarines in particular, were  
112 dominant in soil protist communities of Neotropical forests, findings that suggest those groups  
113 shape animal diversity in forest ecosystems<sup>30</sup>. Similarly, these parasites could contribute to shape  
114 marine animal communities in a marine ecosystem. Their dominance in centuries-old protist  
115 paleocommunities could suggest long-term parasitic pressure over animal communities. Hence,  
116 gregarines may have a trans-ecosystem functional role, and protist paleocommunities, in both soils  
117 and marine sediments, might reveal long-term host-parasite ecological patterns.

118

### 119 **Paleocommunity shifts in relation to coastal pollution**

120 The multivariate regression tree (MRT) analysis suggested that shifts in the protist communities  
121 occurred during the 1930s–40s and 1980s–90s (Figure S3). The protist groups largely responsible  
122 for these shifts were dinoflagellates (Figure 2) and stramenopiles (Figure 3).

123 Dinoflagellate communities drastically changed during the 1940s (break point 1941, BH  
124 core) shifting from the dominance of suessioid genera (*Pelagodinium* and *BiechelerialProtodinium*,  
125 Figure 2) during the entire Middle Age and the XIX<sup>th</sup> century to the beginning of the XX<sup>th</sup> century  
126 to a dominance of gonyaulacoid genera (*Gonyaulax* and *Alexandrium*, Figure 2) during the end of  
127 the XX<sup>th</sup> and beginning of the XXI<sup>th</sup> centuries. Suessioid genera almost disappeared after the 1980s  
128 (1987, DE), they are indeed relatively rare in current coastal plankton<sup>27</sup>, and peridinioid genera  
129 became more important (Figure 2). Changes in the relative importance of the genus *Gonyaulax*  
130 largely explain dinoflagellate variations. The genus *Gonyaulax* progressively decreased in  
131 importance after the 1980s (1987, DE) and the 1990s (1998, EE), whereas the genera *Heterocapsa*  
132 (peridinioid) and the potentially harmful genus *Alexandrium* increased in importance (Figure 2).  
133 This result confirms previous observations of increased abundance of the toxic species *Alexandrium*  
134 *minutum* revealed by real-time PCR analyses on *seda*DNA from the same DE and EE cores in  
135 parallel with the recrudescence of harmful algal blooms caused by this species over the time in the  
136 Bay of Brest<sup>7</sup>.

137 Stramenopiles also drastically shifted during the 1940s and 1950s (Figure 3). The  
138 heterotrophic group MAST (MARine STRamenopiles<sup>31</sup>) and in particular the MAST-12 clade  
139 dominated stramenopile paleocommunities during the Middle Age and the XIX<sup>th</sup> century (Figure  
140 3). The relative abundance of Bacillariophyta (diatoms) started to increase during the XX<sup>th</sup> century  
141 (1942, DE) and dominated after the 1950s (1952, BH) with MAST-12 progressively decreasing in  
142 abundances (Figure 3). Within the diatom community, *Chaetoceros* was progressively replaced by  
143 the genus *Thalassiosira* as well as by other unidentified diatoms after the 1990s (1998, EE) (Figure  
144 3).

145 As noted, genera found in pre-war sediments became very rare after the World War II  
146 (WWII) period and conversely current dominant genera were rare in the past. This indicates that

147 the community shifts observed in this study were irreversible at the time scale of our paleogenetic  
148 analyses.

149 To infer potential causes of paleocommunity shifts in the Bay of Brest, contaminants were  
150 analyzed in sediment samples of the BH core. Three groups of heavy metals were discriminated in  
151 sediment samples (non-parametric correlation, Spearman test,  $p < 0.05$ ; Figure 4, Figure S4A,  
152 Figure S4B, Figure S4C) and concentrations of aluminum (Al)-normalized lithium (Li), nickel (Ni),  
153 mercury (Hg), and lead ( $^{206}\text{Pb}/^{207}\text{Pb}$ ) were examined in the sediment samples (Figure 4, Figure  
154 S4D) as representative of each of the three groups. Li normalized concentrations and dynamics  
155 were constant across the studied interval ( $12.9 \pm 0.8 \text{ mg kg}^{-1}$  (mean  $\pm$  SD). Ni had constant  
156 normalized concentrations throughout the core ( $4.8 \pm 0.2 \text{ mg kg}^{-1}$ ) with the exception of two peaks  
157 detected in the years  $1947 \pm 11$  (WWII period) and  $1913 \pm 16$  (WWI period) (concentration increase  
158 of up to 50%,  $9.8 \text{ mg kg}^{-1}$ ) (Figure 4). At  $1936 \pm 12$  (WWII period), a small  $^{206}\text{Pb}/^{207}\text{Pb}$  peak was  
159 also detected. Hg increased its normalized concentrations from  $1958 \pm 9$  to more recent times  
160 (surface layers) with a peak at  $1981 \pm 5$  (Figure 4). To evaluate whether pollutant sources were of  
161 an anthropogenic origin, the relative enrichment factor (EF) was calculated for every trace metal.  
162 The two concentration peaks observed at  $1947 \pm 11$  for Ni (Figure 4) and Cr (Figure S4B)  
163 correspond to a significant anthropogenic impact (EF = 2.0 for Ni). The EF and concentrations of  
164 Hg (Figure 4) and other trace metals of group 3 (Figure S4C) progressively increased over time,  
165 with maximum EF values between 1.9 and 9.5. These values demonstrated a moderate to severe  
166 anthropogenic contamination after WWII in this order:  $\text{Zn} < \text{Pb} < \text{Ag} < \text{Cu} < \text{Hg}$ . This post-WWII  
167 pollution dynamics was confirmed by Pb isotope ratios ( $\text{Pb}/\text{Al}$ ,  $^{206}\text{Pb}/^{207}\text{Pb}$ ,  $^{206}\text{Pb}/^{208}\text{Pb}$ , Figure 4,  
168 Figure S4D, Figure S4E) and Polychlorinated biphenyl (PCB) contamination profiles (Figure 4).  
169 The concentration profile of the sum of the seven PCB indicator congeners confirmed the influence  
170 of higher anthropogenic input from the 1950s onward. Indeed, the concentration profile of the sum

171 of the seven indicator congeners showed a progressive increase in PCB contamination from 1958  
172  $\pm 7$  until the peak at 1981  $\pm 5$  following the pattern of the third group of heavy metal (Figure 4).

173 During WWII the town of Brest was under Nazi occupation. Historical documents provide  
174 qualitative information about wartime activities linked to pollution, such as the construction of a  
175 submarine base, industrial army activity, navy traffic, and fuel deposit fires. Historical data are  
176 available about the quantity of bombs dropped on the town of Brest and its bay. The 30,000 tons of  
177 bombs and the 100,000 shells deployed over Brest during WWII and even more intensely during  
178 Ally liberation (Figure S1C) must have polluted the water either directly or indirectly through waste  
179 and detritus collected by river catchments flowing in the coastal waters of the bay. The metal  
180 composition of such bombs and explosives are imprecise or very difficult to retrieve. Yet, it is  
181 interesting that trace metal anomalies, including Pb and Cr, were found in sediment samples to be  
182 coincident with the Japanese aviation bombing of Pearl Harbour, the U.S. navy outpost during the  
183 WWII, on December 7, 1941<sup>32</sup>.

184 Regarding the post-WWII period it is difficult to designate a particular source of metal  
185 contamination and the potential inputs could come from atmospheric depositions (Hg and Pb),  
186 agricultural phytosanitary products (Cu and Zn), and urban waste (polymetallic inputs). PCB  
187 contamination profiles sustain the hypothesis of contaminations of agricultural origin. from the  
188 1950s onward. These profiles in sediment are similar to those of other French human impacted  
189 sites<sup>33,34</sup> or other agriculturally exploited sites<sup>35,36</sup>. A palynological study (pollen grains and  
190 dinoflagellate cysts) carried out on a twin core of the DE allowed direct comparison between the  
191 evolution of landscape, surface water, and human practices on Bay of Brest watersheds and  
192 corroborate the hypothesis of the postwar agriculture contamination<sup>37</sup>. Pollen and dinoflagellate  
193 cyst concentration analyses indicate changes in agricultural practices in the Bay of Brest. An  
194 increase in *Alnus* pollen grain concentrations and shifts between cysts of *Lingulodinium polyedra*  
195 and *Gonyaulax digitale* were synchronous with protist shifts shown in this study. These variations

196 have been associated with the evolution of agricultural practices and the increase in river flow  
197 loading due to the implementation of a new agricultural policy after 1945<sup>37</sup>.

198 Plankton shifts have been evaluated on relatively short time scales since the majority of  
199 plankton long-term series have been initiated from the 1950 onward, with the exception of the  
200 Continuous Plankton Recorder Survey, which started in 1937<sup>38</sup>. Changes in plankton communities  
201 during the 1980s–90s were already observed in the Bay of Brest using microscopy counts. These  
202 shifts were associated with unbalanced nitrogen/phosphorus (N/P) ratios over time and in particular  
203 to the high concentrations of nitrogen in coastal water due to run-offs of agricultural field through  
204 water catchments and rivers<sup>39,40</sup>. To compensate for the gap in pre-industrial plankton data,  
205 researchers have used modeling approaches mostly to evaluate the effect of climate changes on  
206 plankton<sup>41,42</sup>. Traditional sedimentary paleoecological approaches based on microfossil analyses  
207 (spores, diatoms frustules, dinoflagellate cysts, foraminifers and coccoliths, and acritarchs) have  
208 allowed researchers to evaluate shifts on a paleoclimatological time scale, but also community  
209 changes after industrial pollution<sup>37,43</sup>. *SedaDNA* analyses on plankton have shown its potential as a  
210 tool for studying the effect of human perturbation on biological communities<sup>18,43,44,45,46</sup>.  
211 Paleogenetic analyses revealed long-term shifts in plankton sometimes proving the anthropogenic  
212 influence<sup>9,10,12,13,17</sup>, and the irreversibility of those changes<sup>47,48</sup>. *SedaDNA* analyses have  
213 highlighted the increase and recrudescence of harmful algal bloom species in lakes<sup>49</sup> and coastal  
214 waters<sup>7,8</sup> and reflected an increase in eutrophication due to human pressures<sup>9,10,13,17,48,50</sup>. Our  
215 paleogenetic study showed that the cumulative effect of the trace metal and PCB pollution of the  
216 WWII and the postwar periods caused drastic changes in paleocommunity compositions, especially  
217 for dinoflagellates and stramenopiles, and the variations in dominant genera within these groups  
218 after the 1980s and 1990s. The effect of punctual or long-term contaminations from heavy metals  
219 (including Pb, Ni, and Cr) and PCBs are known to affect coastal plankton community  
220 composition<sup>51,52</sup> and to have a negative effect on phytoplankton species development<sup>53</sup>, including

221 dinoflagellates<sup>54,55</sup>. The occasional and chronic human impacts occurred during the WWII and post-  
222 war period resulted in unstable and non-resilient variations of protistan communities the Bay of  
223 Brest over the last 70 years. Hence, this study demonstrates the potential irreversible consequence  
224 of multiple and cumulated pollutions over the microbial compartment of the coastal ecosystem.

225         What defines healthy coastal ecosystems is under debate. The main issue is whether natural  
226 systems are in balance and if they tend to return to that balance when perturbed or whether  
227 ecosystems are dynamic systems that are transient and unstable<sup>1</sup>. The bottleneck of such analysis is  
228 the contemporary acquisition of baselines of pristine ecosystem conditions and post-perturbation  
229 analyses. The comparative analysis of past versus modern ecosystem conditions may help to  
230 establish or optimize ecosystem strategies<sup>4</sup>. This study highlights the importance of retrospective  
231 analyses for the evaluation of coastal ecosystem stability and resilience and the relevance of  
232 paleogenetic data for these analyses. The impact of short- and long-term chronical pollution is  
233 demonstrated here on the microeukaryotic planktonic communities, a key compartment in marine  
234 ecosystems. Shifts in this compartment might cause cascading effects on other biological  
235 components of the ecosystem affecting the whole marine food web. These findings can further  
236 sustain the use of the paleoecological approach for the development of restoration efforts and policy  
237 actions aiming at a sustainable management of coastal areas.

238

### 239 **Acknowledgments**

240 Research funds were provided by the Brittany Region (Région Bretagne) as part of the  
241 *Paleoecology of Alexandrium minutum dans la Rade de Brest–Marché* n°2017-90292 project  
242 PALMIRA, which supported the core sampling, analyses, and post-doc fellowship of MAssudrie.  
243 Analyses were also funded by the initiative Ecosphere Continentale et COtière (EC2CO) of the  
244 *Institut National des Sciences de l’Univers/Centre Nationale de la Recherche Scientifique*:  
245 PALMITO (2013–2015) and CA’MOMI (2015–2017) projects. We thank Arnaud Marrec and

246 Yannick Fagon (Région Bretagne – Service Ingénierie de la Direction des Ports), who allowed the  
247 implementation and progression of PALMIRA. We are grateful to all members of the crew of the  
248 N/O *Thalia* ship of Ifremer for providing technical expertise in sediment core collection. We thank  
249 Angélique Roubi and Jérémie Gouriou of the laboratory GM/LGS of Ifremer for helping during  
250 onboard core sampling. We acknowledge our colleagues from the laboratory DYNECO/Pelagos  
251 and of Ifremer (Françoise Andrieux, Annie Chapelle, Cécile Jauzein, Mickaël Le Gac, Martin Plus,  
252 Sophie Schmitt, and Agnès Youenou) for their assistance during core subsampling. We are warmly  
253 grateful to Lauriane Madec (Ifremer), Khadidja Z. Klouch (a PhD student supervised by RS from  
254 2012 to 2016), and Laure Guillou (CNRS, Station Biologique de Roscoff, France) for their initial  
255 contribution to the EE and DE core analyses. We thank Stéphane Lesbats and Olivier Dugornay of  
256 Ifremer’s Audiovisual Service for onboard collection and scuba diving images of the sampling and  
257 for producing videos for the project. We thank colleagues from the Ifremer PFOM/LPI laboratory  
258 for having provided clean laboratory facilities and Darryl Perree for technical assistance in genetic  
259 analyses. We acknowledge the historical archive personnel of Brest and Quimper and in particular  
260 Hugues Courant, Isabelle Knab-Delumeau (Ecole Navale de Brest), and Yves Coativy (University  
261 of Brest) for their help in the analyses of historical information of the Bay of Brest. Muriel Vidal is  
262 acknowledged for her contribution to the rational and analysis of the work. We are warmly grateful  
263 to Isabelle Domaizon (INRAE) for helpful discussion during the entire project. R.S., M.L., and  
264 K.N.M. are part of GDR PHYCOTOX, a CNRS/IFREMER French national network on Harmful  
265 Algal Blooms.

266

#### 267 **Author contributions**

268 R.S. designed and performed the research, conceived and carried out sampling, analyzed results  
269 and data, and wrote the paper. M.Lassudrie performed DNA extraction, genetic analyses, analyzed  
270 results, and contributed to writing. P.C., C.N., and L.Q. contributed to metabarcoding biostatistical

271 analyses. P.D. curated the data depositary. N.B. and V.L. performed, respectively, heavy metal and  
272 PCB analyses; analyzed results; and contributed to writing. S.S. carried out sediment dating and  
273 contributed to writing. A.E. helped in core sampling realization, carried out granulometry analyses,  
274 and contributed to writing. K.N.M., C.L., and A.P. contributed to paleoecological data analyses and  
275 interpretation. M.L. and J.Q. technically supported sampling and genetic analyses.

276

### 277 **Declaration of interests**

278 The authors declare no competing interests.

279

### 280 **Figure legends**

281

282 **Figure 1. Paleocommunity diversity.** Eukaryotic diversity composition of the BH core of the Bay  
283 of Brest inferred by metabarcoding of the V7 (left panel) and V4 (right panel) 18S rDNA  
284 of *seda*DNA extracted from Medieval to contemporary sediments. Eukaryotic lineages are  
285 listed and color tones are used to indicate eukaryotic groups.

286

287 **Figure 2. Shifts in dinoflagellate community composition.** Dinoflagellate diversity analyses  
288 inferred from the V4 metabarcoding data of the TOT *seda*DNA of the BH, DE, and EE cores  
289 of the Bay of Brest. Core dinoflagellate orders are identified with color tones (red:  
290 Gonyaulacales; yellow: Peridiniales; blue: Gymnodiniales; green: Suessiales; violet:  
291 Dinophysales). The dinoflagellate sister clades of marine alveolate (MALV) groups I, II,  
292 and III are also represented. Unidentified dinoflagellates are classified as Unknown. The  
293 multivariate regression tree analysis suggested dates of chronological partitioning of the  
294 data, representing shifts in community composition, and identified the dinoflagellate group  
295 mostly explaining these shifts. Only the first and major complexity level is represented. The

296 genus *Gonyaulax* (Gonyaulacales) is responsible for 100% of the deviance in the break point  
297 identified in 1941 for BH (complexity: 35.6), for 43% of the deviance in the break point  
298 identified in 1987 for DE (complexity: 42.1), and for 77% of the deviance in the break point  
299 identified in 1998 for EE (complexity: 33.7). See also Figures S2 and S3.

300  
301 **Figure 3. Shifts in stramenopile community composition.** Stramenopile diversity analyses  
302 inferred from the V4 metabarcoding data of the TOT *sead*DNA of the BH, DE, and EE cores  
303 from the Bay of Brest. Stramenopiles groups are identified with color tones (red: phylum  
304 Bacillariophyta [diatoms]; green: phylum Dictyochophyta; yellow: phylum Labyrinthulea;  
305 blue: marine stramenopiles [MAST]; violet: Oomycota; other colors: clades with *incertae*  
306 *sedis* classifications). Unidentified stramenopiles are classified as Unknown. The  
307 multivariate regression tree analysis suggested dates of chronological partitioning of the  
308 data, representing shifts in community composition, and the identified stramenopile group  
309 mostly explains these shifts. Only the first and major complexity level is represented. The  
310 diatom genus *Chaetoceros* is responsible for 93% of the deviance in the break point  
311 identified in 1952 for BH (complexity: 19.5) and 100% of the deviance in the break point  
312 identified in 1998 for EE (complexity: 33.7). The group MAST-12A is responsible for 100%  
313 of the deviance in the break point identified in 1942 for DE (complexity: 63.0)

314  
315 **Figure 4. Pollutant temporal variations.** Pb isotope ratio and selected heavy metal and PCB  
316 concentrations in the BH core of the Bay of Brest. The Al-normalized dynamics of Li, Ni,  
317 and Hg are representative of three groups of analyzed heavy metal. The cumulative  
318 concentrations of the seven measured indicator PCB congeners (CB28, 52, 101, 118, 138,  
319 153, 180) are indicated as  $\Sigma$ 7PCBs. See also Figure S4.

321 **STAR Methods section**

322 **Resources Availability**

323

324 **Lead Contact**

325 Further information and requests for resources and reagents should be directed to and will be  
326 fulfilled by the Lead Contact, Raffaele Siano (raffaele.siano@ifremer.fr).

327

328 **Materials availability**

329 This study did not generate new unique reagents.

330

331 **Data and code availability**

332 All data needed to evaluate the conclusions of the paper are presented in the paper and/or in the  
333 Supplementary Material. Raw Illumina-Miseq data used for metabarcoding analyses have been  
334 submitted to NCBI (<https://www.ncbi.nlm.nih.gov>) with the data reference number PRJNA667629  
335 (BH data) and PRJNA680674 (DE and EE data).

336

337 **Experimental model**

338 **Study area**

339 The Bay of Brest (Brittany, France, northeast Atlantic) is a semi-enclosed coastal ecosystem  
340 connected to the Iroise Sea (Atlantic Ocean) by a narrow (2 km) and deep (50 m) strait (Figure  
341 S1A). The bay is a shallow macrotidal coastal ecosystem with 50% of its surface deeper than 5 m.  
342 It is characterized by coarse sediments in deep waters and fine and muddy sediments in the upstream  
343 part of the estuaries. The majority (80%) of freshwater inputs come from two main rivers: the Aulne  
344 River (1842 km<sup>2</sup>) in the southeastern part and the Elorn River (402 km<sup>2</sup>) in the northeastern part of  
345 the Bay. The Brest area experienced a progressive development from the Antiquity through the

346 Middle Ages during the Duchy of Brittany, but it became a real naval town during from the XVII<sup>th</sup>  
347 to XVIII<sup>th</sup> centuries with the construction of the naval harbor. During this time, the population and  
348 the naval activity increased progressively. Then, after a lull of almost a century, Brest experienced  
349 a second industrial development from the end of the XVIII<sup>th</sup> century until WWI. In 1940, the  
350 German army conquered Brest and built the famous submarine base in only three months. The base,  
351 the coastal area, and the whole town were bombed continuously by the Allies until 1945, with more  
352 than 30000 tons of bombs deployed (Figure S1C). The town of Brest was completely destroyed,  
353 with 965 people killed and 740 injured. During this period, the coastal area was the receptacle of  
354 heavy pollution due to the industrial army activity, navy traffic, and fires of French fuel deposits  
355 practiced by the German army on the land. The town of Brest was liberated on September 19, 1944,  
356 after 45 days of heavy fighting. After the liberation, the town and the harbor started their  
357 reconstruction. In 1947, the explosion of the Ocean Liberty vessel provoked grave damage to the  
358 entire town and the coastal area, with more than 3000 tons of the heavily explosive fertilizer  
359 ammonium nitrate released in the harbor's waters. Since 1950, the Brest area has undergone an  
360 intensive agricultural industrial development: the urban area increased and the harbor extended over  
361 the sea. During this period and until the 1990s, the area had experienced several changes in the  
362 anthropogenic loading of nutrients; with an increase in nitrogen supply due to the development of  
363 anthropogenic activities, and near the end of that period, a decrease in phosphorous supply resulting  
364 from the ban of washing powders containing orthophosphates<sup>56</sup>. Consequently, a significant  
365 imbalance in the nitrogen/phosphorus ratio<sup>57</sup> altered the composition of planktonic and benthic  
366 communities<sup>39,40,58</sup>. After the 1990s, the agricultural policy of the region has tried to control  
367 eutrophication of the area, and since then the nutrient loading has progressively decreased in the  
368 coastal area of the Bay of Brest.

369

## 370 **Core sediment sampling**

371 Biological analyses were inferred from three sediment cores collected in the Bay of Brest. Two  
372 interface cores were collected by a gravity corer at the main estuaries' outlets of the Bay of Brest:  
373 the Elorn Estuary (EE: 48°23'46.79"N, 4°23'2.01"W; December 11, 2012; 12 m depth; core length  
374 31 cm) and the Daoulas Estuary (DE: 48°20'46.6"N, 4°17' 41.20"W; May 21, 2014; 3 m depth; core  
375 length 58 cm) (Figure S1A). A third core was collected near the Brest Harbor in a non-dredged  
376 zone (BH: 48°22'52.74"N, 04°26'54.60"W; April 25, 2017; 7.10 m depth; core length 344 cm) on-  
377 board the N/O *Thalia* using a Kullenberg core sampler (Figure S1A; Video S1). Dating was  
378 obtained from a twin core collected at the EE (see<sup>7</sup> for details of methods) and from the same cores  
379 used for biological analyses at DE and BH. Immediately after sampling, sediment cores were  
380 delicately extruded and sliced into 1 cm thick layers (Video S1). Due to its length, the BH core was  
381 previously separated into four sections of equal length. For EE and DE interface cores, every 1 cm  
382 layer was collected and analyzed. For the long BH core, only one in two slices was used for  
383 subsampling and further analyses to avoid contamination across sample layers. To further avoid  
384 contamination by smearing between layers during the core extraction, only the inner part of each  
385 slice was subsampled, using sterile 6 cm diameter Petri dishes and sterilized wooden tongue  
386 depressors (Video S1). Sterile, new equipment was used to sample each layer. Samples collected  
387 in a Petri dish for genetic analyses (about 10 g of wet sediment) were preserved in plastic 50 mL  
388 deoxygenated cryotubes, immediately frozen in liquid nitrogen, and then stored in a -80°C freezer  
389 until further analyses. Samples for granulometry, organic carbon, heavy metals, and PCB  
390 compounds were collected from the same layers of DNA samples, whenever possible, or from the  
391 discarded layer not used for genetic analyses. For organic carbon analysis, samples were frozen at  
392 -20°C and then lyophilized before analysis. Other sediment aliquots were stored at 4°C and in the  
393 dark until further analysis.

394

## 395 **Method details**

## 396 **Sediment dating and granulometry**

397 Dating of recent sediments (< 150 years) was established for the Elorn Estuary (EE), Daoulas  
398 Estuary (DE) and Brest Harbour (BH, KS06) cores using depth profiles of excess  $^{210}\text{Pb}$  ( $^{210}\text{Pb}_{\text{xs}}$ ,  
399 lead), a naturally-occurring radionuclide, and  $^{137}\text{Cs}$  (cesium), an artificial radionuclide. The  
400 chronology of DE and EE were previously described by Klouch et al.<sup>7</sup>. The EE and DE cores  
401 covered, respectively, about 72 cal. yr. (calendar year) (from  $1939 \pm 2$  to  $2011 \pm 1$  AD) and 99 cal.  
402 yr. (from  $1915 \pm 7$  to  $2014 \pm 1$  AD) (Data S1A, Data S1B). The BH core is here described for the  
403 first time (Figure S1B, Data S1C) and covers the longest time period from  $2928 \pm 94$  BC ( $4878 \pm$   
404  $94$  BP) to  $2015 \pm 1$  AD, i.e., about 5000 cal. yr.

405 For the BH core activities ( $\text{mBq g}^{-1}$ ) of  $^{210}\text{Pb}$ ,  $^{226}\text{Ra}$  (radium), and  $^{137}\text{Cs}$  were measured in  
406 ~10 g of dry sediment using Broad Energy Germanium  $\gamma$  detector (BEGe, Mirion Technologies,  
407 France). The presence of shell fragments and maerl made gamma measurements difficult. First, the  
408 coarse carbonate fraction was sorted and removed. The remaining fine carbonate fraction diluted  
409 the radioelement contents, which implies long counting times ranging from 24 to 126 hours per  
410 sample. The detector was calibrated using certified reference material from the International Atomic  
411 Energy Agency (RGU-1; SOIL-6). Excess  $^{210}\text{Pb}$  ( $^{210}\text{Pb}_{\text{xs}}$ ) was calculated as the difference between  
412 the measured  $^{210}\text{Pb}$  and  $^{226}\text{Ra}$  activities. Activity errors were based on 1 SD counting statistics and  
413 propagated for  $^{210}\text{Pb}_{\text{xs}}$ . The two first layers of the core were measured twice a few days and several  
414 months after sampling to determine excess  $^{234}\text{Th}$  (thorium), a short-lived radionuclide ( $T_{1/2} = 24.1$   
415 days), which is a tracer of a good recovery of the uppermost sediment and of bioturbation. Activities  
416 of  $^{210}\text{Pb}_{\text{xs}}$  present an exponential decrease from the top of the core to negligible values below 20  
417 cm. This rapid decrease and the absence of a mixed layer in the upper section of the  $^{210}\text{Pb}_{\text{xs}}$  profile  
418 testify to the absence of significant mixing of the sediment. The long-lived and naturally-occurring  
419  $^{232}\text{Th}$  is usually associated with the detrital fraction; therefore, the rather constant  $^{232}\text{Th}$  activity in  
420 the BH core indicates the absence of changes in lithological sources or proportions. This implies

421 that the changes in  $^{210}\text{Pb}_{\text{xs}}$  activities with depth are mainly related to time (radioactive decay of  
422  $^{210}\text{Pb}$  according to its half-life of 22.3 years) and are suitable to estimate sedimentation intensity.

423 The constant flux and constant sedimentation (CF–CS) model were used to calculate a mean  
424 sedimentation accumulation rate of  $0.23 \pm 0.040 \text{ cm yr}^{-1}$  from the  $^{210}\text{Pb}_{\text{xs}}$  profile. The DE and EE  
425 cores have higher mean sediment accumulation rates due to fluvial sediment inputs (EE:  $0.44 \text{ cm}$   
426  $\text{yr}^{-1}$ ; DE:  $0.41 \text{ cm yr}^{-1}$ ) than the BH core. For BH the ages of the sediment layers were calculated  
427 using the sedimentation rate and assuming the age of the top sediment to be 2015. The  $^{137}\text{Cs}$   
428 activities are low but present an onset at about 16 cm, which corresponds to the first introduction  
429 of this artificial radionuclide in the environment in the early 1950s and validates the chronological  
430 framework based on  $^{210}\text{Pb}_{\text{xs}}$  (Figure S1B).

431 Dating of ancient sediments ( $> 150$  years) for BH was performed by analyzing  $^{14}\text{C}$  in eight  
432 gastropod shells (*Bittium* spp., *Crisilla* spp., *Hydrobia* spp., *Jujubinus* spp., and *Rissoa* spp.; total  
433 weight of each sample  $< 10 \text{ g}$ ) collected from the sieved sediment. The remaining material of five  
434 of these samples was not enough to perform genetic extractions.  $^{14}\text{C}$  analyses were conducted at the  
435 Poznań Radiocarbon Laboratory (Poznań, Poland). Absolute dating was corrected for the mean  $^{14}\text{C}$   
436 age difference between the atmosphere and oceanic surface waters by applying a reservoir  
437 correction (R) of 325 years with an applied regional deviation (DR) for the bay of Brest of 46 years.  
438 The results of absolute dating were then calibrated using Calib Rev 7.0.4 software from the  
439 “Intcal13” calibration curve<sup>59</sup>, with a confidence level of 95% for the SD (sigma 2). There was no  
440 dating inversion for the eight analyzed samples; however, the  $^{14}\text{C}$  results showed two important  
441 time gaps in dating (Data S1C). The former concerns the gap between 32 and 82 cm below the  
442 seabed surface separating the recent sedimentation developed from the middle of the XIX<sup>th</sup> century  
443 ( $1879 \text{ yr.} \pm 21 \text{ AD}$ ), estimated by  $^{210}\text{Pb}_{\text{xs}}$ , and old deposits dated from the central middle age ( $530$   
444  $\pm 108 \text{ AD}$  to  $874 \pm 111 \text{ AD}$ ). Additional sediment analyses on other cores (data not shown) showed  
445 that this gap is less important and may have occurred between 1000 AD and 1350 AD. This time

446 offset is recorded for all the conserved sediment deposits in the bay of Brest. This period is well  
447 known to be a warm climatic sequence called the Medieval Warm Period (MWP) characterized by  
448 recurring winter successive storms<sup>59</sup>, at the origin of the construction of aeolian dune systems on  
449 the North Atlantic Ocean coasts. The second time gap separates the Middle Ages from the Egyptian  
450 period, more precisely corresponding to the Third Intermediate Period until the Early Dynastic  
451 Period. It represents a seismic unconformity surface ranging from  $2025 \pm 129$  BP to  $3184 \pm 164$   
452 BP<sup>59</sup> and corresponds to be a typical geological transition characterizing a precise step of the marine  
453 transgression and called the maximum flooding surface (MFS). The coarse deposits between 213  
454 and 233 cm in the core associated with this time gap result of a high-energy marine environment  
455 that was able to erode underlying sand Egyptian age deposits.

456 For sediment granulometry, particle size analyses were carried out with a laser diffraction  
457 system for the sediment fraction below 2 mm. The percentages of the main sedimentary classes  
458 (gravel, sand, silt, and clay) were thus determined for each level sampled with the Gradistat package  
459 developed by Gregoire et al. (see<sup>60</sup> for methods). All cores mostly comprised a mix of clay, silt, and  
460 fine sand particles; the BH core was  $4 \pm 4\%$  clay,  $43 \pm 9\%$  silt, and  $36 \pm 8\%$  fine sand particles  
461 (mean  $\pm$  standard deviation [SD]). However, in the lower part of the BH core, below 204 cm, the  
462 sand and detritic gravel sediment fraction increased to represent more than 80% of the total  
463 sediment sampled.

464

#### 465 ***seda*DNA extraction and amplification**

466 Genomic DNA extraction was carried out from 3–10 g of wet sediment from each of the 31 and 58  
467 layers, respectively, of the EE and DE cores, and from 46 layers of the BH core (Table S1). In  
468 marine sediments, given the importance of resting stages—which protect DNA inside the cells—it  
469 was hypothesized that intracellular DNA constitutes the highest proportion of the total *seda*DNA  
470 extracted with classical protocols used for soil matrices, such as in the DNeasy PowerMax Soil Kit

471 (Qiagen). This hypothesis was tested on the BH samples. For each of the 46 sediment layers of BH,  
472 three different extraction protocols were applied to extract respectively: (1) total DNA (TOT)  
473 (DNeasy PowerMax Soil Kit as per the manufacturer instructions); (2) intracellular DNA (IN) from  
474 resting stages<sup>61</sup>, by eliminating extracellular DNA through washing and heating steps before DNA  
475 extraction using the DNeasy PowerMax Soil Kit); and (3) extracellular DNA (EX) (following  
476 methods used in terrestrial ecological biodiversity surveys<sup>24</sup>, which comprises extracting  
477 extracellular DNA in saturated phosphate buffer prior to using the DNeasy Power Max soil kit  
478 without the cell lysis step).

479 All *seadaDNA* extractions and manipulations were performed to avoid cross-contamination  
480 between samples or with modern DNA, by following specific instructions for working with aDNA  
481 and specifically for marine *seadaDNA*<sup>5,22,62</sup>. Extractions were carried out in an isolated, specific  
482 clean laboratory adapted to aDNA extraction, under a laminar flow cabinet (Video S1). One  
483 sediment layer was extracted at a time, all the surfaces and material used were carefully  
484 decontaminated between each sample treatment using chlorine or DNA-away™ (Thermo Fisher),  
485 and the laminar flow cabinet was also decontaminated with ultraviolet light. The analyst wore  
486 dedicated clothing and disposable personal protective equipment including a lab coat, gloves, and  
487 a facemask that were changed between each sample (Video S1). Blanks (no template controls) were  
488 extracted to check for the absence of contamination from the working area and from kit reagents.  
489 DNA extracts were immediately stored in a dedicated -80°C freezer. DNA was quantified with the  
490 Quant-iT™ PicoGreen® dsDNA assay (Invitrogen).

491 IN *seadaDNA* extractions yielded a DNA concentration close to that of total TOT *seadaDNA*  
492 extractions all along the BH core (Figure S2A, Figure S2B), whereas EX *seadaDNA* extractions  
493 yielded a constant, low DNA concentration all along the core (Figure S2A, Table S1). There were  
494 higher concentrations at superficial core layers in TOT and IN fractions (5 cm depth; max 4971.61  
495 ng DNA g<sup>-1</sup>), then a rapid decrease in concentrations down to 19 cm depth (max 761.64 ng DNA

496  $\text{g}^{-1}$  in TOT). There were constant TOT and IN *sedaDNA* concentrations from 19 to 222 cm depth  
497 (respective averages  $\pm$  standard deviation:  $697 \pm 135$  and  $566 \pm 113$  ng DNA  $\text{g}^{-1}$ ). From 231 cm to  
498 the end of the core, TOT and IN *sedaDNA* concentrations decreased considerably ( $278 \pm 80$  and  
499  $239 \pm 94$  ng DNA  $\text{g}^{-1}$ , Figure S2A). This section of the core corresponded to coarser (sandy)  
500 sediment granulometries compared with the rest of the core. Such a sediment type is less favorable  
501 to DNA preservation, which probably explains the DNA concentration drop observed in this part  
502 of the core (Figure S2A). In the light of results obtained for these samples, only the total DNA  
503 extraction protocol was used for EE and DE extractions. The comparison of different DNA  
504 extraction methods showed that the DNA concentrations in sediments along the BH core were  
505 similar when comparing total *sedaDNA* (TOT) and intracellular *sedaDNA* (IN) extracts, whereas  
506 the concentration was much lower in the extracellular *sedaDNA* (EX) extracts (Table S1).

507 To analyze possible *sedaDNA* degradation by fragmentation and to check the possibility  
508 and reliability of the amplification of  $> 300$  bp DNA fragments from ancient marine sediments,  
509 metabarcoding analyses of the V4 (ca. 390 bp) and V7 (ca. 260 bp) hyper-variable regions of the  
510 18S rRNA gene were compared for BH samples. The V4 region is commonly used in protist  
511 biodiversity survey<sup>27,50</sup>, whereas the V7 barcode has been suggested as a useful paleogenetic  
512 barcode in paleolimnological studies<sup>13</sup>, although it had not been tested in marine paleogenetic  
513 approaches. The V4 and V7 regions were amplified in samples and extraction using respectively  
514 the eukaryotic primers TAREuk454FWD1 and TAREukREV3<sup>27</sup> and 960F et NSR1438<sup>13</sup> assembled  
515 with the GeT-PlaGe adaptors from GeT sequencing platform (Toulouse, France,  
516 <http://get.genotoul.fr>) for Illumina Mi-Seq sequencing. For both amplifications, the reaction  
517 mixture was prepared in a final volume of 50  $\mu\text{L}$ , containing 0.02 U  $\mu\text{L}^{-1}$  Phusion High Fidelity  
518 DNA polymerase and 1X Phusion High-Fidelity Buffer (NEB), 0.2 mM dNTP mix, 0.4  $\mu\text{M}$  of each  
519 primer, 3% dimethyl sulfoxide, 2  $\mu\text{L}$  DNA template, and DNA-free water. Extraction blanks were  
520 also amplified, and positive controls (mock protist community composed of five different species

521 of microalgae) and negative controls (without DNA templates) were used to check the efficiency  
522 and specificity of the PCR. The following cycling program was used for V4: an initial denaturation  
523 step at 98°C for 30 s, 14 cycles of 98°C for 10 s, 53°C for 30 s, and 72 °C for 30 s; 21 cycles of  
524 98°C for 10 s, 48°C for 30 s, and 72°C for 30 s; and a final elongation step at 72°C for 10 min. The  
525 cycling program for V7 was: an initial denaturation step at 98°C for 30 s; 35 cycles of 98°C for 10  
526 s, 55°C for 30 s, and 72°C for 30 s; and a final elongation step at 72°C for 10 min. PCR products  
527 were checked on a 1.5% agarose gel (1× Tris-borate-ethylenediaminetetraacetic acid and Gel Red).  
528 Three replicates reactions per sample were run and PCR products were pooled and sent to GeT  
529 sequencing platform, where they were purified and checked for quality and quantity using a  
530 fragment analyzer. PCR products yielding an insufficient DNA concentration of the expected  
531 fragment size were excluded (extraction blanks, 3 EE samples, 27 DE samples, 7 EX DNA, and 1  
532 IN DNA for the V4 region in BH samples). Four libraries were built, keeping separate the samples  
533 from different cores and the different regions (V4 and V7), for sequencing from both sides using  
534 an Illumina MiSeq (2 × 250bp for V4 and 2 × 150bp for V7). As for the BH core, for the V4 region  
535 the range number of reads obtained after sequencing were: 13 812 to 143 391 (TOT), 32 487-  
536 118 101 (IN), and 7 566-129 794 (EX). For the V7 region the range number were: 2 585 to 72 950  
537 (TOT), 1 795-73 061 (IN), and 997-112 916 (EX). For the EE and the DE core the V4 read number  
538 range were respectively: 32 734-425 286 and 37 471-236 421.

539

#### 540 **Metabarcoding analyses**

541 Sequenced data of the V4 (BH, DE and EE) and V7 (BH) 18S rDNA were submitted to quality  
542 checking by FastQC coupled with MultiQC. Primers and adapters have been removed in forward  
543 and reverse file separately with Cutadapt v1.18<sup>63</sup> using the "--discard-untrimmed" argument, which  
544 discards reads without target primers. BBmap v38.22 was used to reorder reads and eliminate  
545 singletons from each pair with the repair function. Sequence filtering and trimming as well as

546 Amplicon Sequence Variant (ASV) inference were carried out using the DADA2 strategy with the  
547 DADA2 R package and using the default parameters<sup>64</sup>. Taxonomic assignment of ASV was  
548 performed on the basis of the naive Bayesian RDP methodology with the database PR<sup>2</sup> v4.11<sup>65</sup>.  
549 Finally, metadata files (sample ID, sediment layer dept, type of DNA extraction, and taxonomy)  
550 was separately created for each sediment core (BH, DE, and EE). There was a second data cleaning  
551 to remove ASVs identified as contamination (e.g., ASVs assigned to *Homo sapiens* or *Capra*  
552 *hircus*). For diversity and ecological studies, ASVs with relative abundances < 0.0% for the V4  
553 dataset and < 0.006% for the V7 dataset were removed from the databases using the R package  
554 phyloseq. This step allowed us to eliminate rare ASVs and further sequence errors and to analyze  
555 > 90% of total ASV richness for each database (Table S2). After this step, samples 1-4 (6 cm depth)  
556 and 1-6 (8 cm) of the BH core were eliminated from the V4 and V7 database because the observed  
557 richness value was too low. To compare samples, V4 and V7 data of all cores were normalized by  
558 a rarefaction method, which comprises a random subsampling of the data by a hypergeometric law.  
559 A normalization threshold was established on the basis of rarefaction curves (Figure S2F) modeled  
560 using the function ggrare deriving from the function rarecurve of the vegan R package with the  
561 argument “step=100”<sup>66</sup>. The phyloseq R package rarefy\_even\_depth was used for data  
562 normalization<sup>67</sup>. For BH, only samples from the surface to 231 cm, used for diversity and ecological  
563 analyses, were normalized. For DE and EE, all samples were normalized.

564 Comparative diversity patterns emerged between TOT and IN with both V7 and V4 18s  
565 rDNA  $\beta$  diversity analysis. For both barcodes, the highest number of ASV were found (in both  
566 absolute number and percent over the total ASV number) with the IN DNA extraction method,  
567 throughout the whole core (Table S2). The highest ASV number (both in absolute number and  
568 percent over the total ASV number) were found in the middle section of the core (from 148 to 160  
569 cm) during the Middle Ages (Figure S2C). There were progressive decreases in diversity toward  
570 the upper section of the core (more recent times) and the deeper layers (more ancient times) (Figure

571 S2C). Sample assemblages ( $\beta$  diversity, analysis based on the Jaccard diversity index) were similar  
572 between TOT and IN. EX samples differed in ASV composition (Figure S2D). Embryophyta  
573 (plants) and Unknown ASVs were preferentially amplified in EX samples. BH sediment sample  
574 layers could be separated into two groups according to both amplicon sequence variant (ASV)  
575 richness and  $\beta$  diversity the first including layers from 2 to 231 cm, and the second composed of  
576 deeper core layers, from 233 to 340 cm, with lower ASV richness (Figure S2D). The rarefaction  
577 curves for each sample showed different TOT and IN richness saturation according to the core layer  
578 depth (Figure S2F). The decrease in ASV diversity and DNA concentration in the lower part of the  
579 core was associated with a different sediment granulometry. *SedaDNA* likely had been better  
580 preserved in the silty–muddy sediments of the upper part of the core than in the coarse sediments  
581 of the lower part. Given these differences, we could not compare the DNA archives of the lower  
582 part of the BH core (233–340 cm) to the more recent ones. Therefore, we performed further analyses  
583 of protist diversity using normalized data from the upper part of the core only (3–231 cm), which  
584 covered a period of ca. 1400 years (including the Anthropocene period), from the Middle Ages  
585 (V<sup>th</sup>–VI<sup>th</sup> centuries) to the contemporary era (XXI<sup>th</sup> century).

586 Most of the ASV obtained with the TOT *sedaDNA* extraction method were common to  
587 those obtained with the IN *sedaDNA* when considering the  $\geq 1\%$  abundant protist ASVs, with on  
588 average 69% and 58% of TOT ASVs common to IN when using the V7 and V4 barcodes,  
589 respectively (Figure S2E). These values increased to 76% (V7) and 65% (V4) when considering  
590 only ASVs from the surface to 231 cm (Figure S2E). In the lowest part of the core most of the  
591 ASVs that are not in common between IN and TOT were only amplified with TOT extraction  
592 method. Over the entirety of the core, 83% (V7) and 82% (V4) of these common ASVs were  
593 assigned to protist genera known to include species that can produce resting stages (Data S2).

594

## 595 **Pollutant analyses**

596 Heavy metal and PCB analyses were carried out on 12 sediment samples of the BH core, covering  
597 the period of the industrial revolution of the XIX<sup>th</sup> century to contemporary times (AD 2003 ± 2).  
598 Pollutant analyses were carried out on the same samples used for genetic analyses when enough  
599 material was available. Whenever necessary, additional samples of lower or upper sediment layers  
600 were exploited. For heavy metals, further control analyses were performed on more ancient  
601 sediments. All reagents, labware acid cleaning, and solution dilutions for elemental and isotope  
602 analyses were performed using 18.2 MΩ.cm<sup>-1</sup> H<sub>2</sub>O (Nanop System®) and ultra-pure acids  
603 (PlasmaPure Plus grade, SCP science®). Unsieved dry aliquots of sediments were digested in  
604 Teflon® bombs on a coated graphite block using a multiple-step acid procedure with hydrofluoric  
605 acid, hydrochloric acid, and nitric acid. The final extract solution was split for subsequent elemental  
606 and isotope analyses. Procedural blanks and international certified reference materials (MESS-3  
607 from NRC – CNR®) were processed in each batch of sediment samples and followed the complete  
608 procedure (digestion, elemental analysis and isotope measurements). Elemental concentrations of  
609 Ag, Al, Cd, Co, Cr, Cu, Fe, Hg, Li, Mn, Ni, Pb, V, and Zn were determined by inductively coupled  
610 plasma mass spectrometry (Q-ICP-MS, iCAP Q, Thermo Fisher Scientific). The accuracy,  
611 indicated by average bias, was always within 10% of the certified values of reference material for  
612 the considered elements. The Pb isotope ratio (<sup>206</sup>Pb/<sup>207</sup>Pb and <sup>206</sup>Pb/<sup>208</sup>Pb) measurements were  
613 performed with the same Q-ICP-MS equipment. Mass bias and instrumental drift were corrected  
614 with a standard bracketing method using the NIST SRM-981 standard reference material. The  
615 <sup>206</sup>Pb/<sup>207</sup>Pb and <sup>206</sup>Pb/<sup>208</sup>Pb internal relative SD averages were 0.15 ± 0.05% and 0.47 ± 0.13% (1s,  
616 n = 20), respectively.

617 To compare particle results from different locations with variable physical and chemical  
618 composition, a normalization procedure is commonly applied. The dilution effects related to grain  
619 size and mineralogical heterogeneities were decreased by the normalization of the Al concentration  
620 in the sample to the concentration of a reference element. Al was used as the reference element for

621 the particulate material due to (i) its conservative behavior in the core; (ii) its characterization of  
622 the clay-size fraction, which is enriched with most trace elements; and (iii) its very low sensitivity  
623 to human activities. Normalized metal concentrations were obtained by dividing the concentration  
624 of the studied element by the concentration of a normalizer element in the same sample (X in  
625 Equation 1). Normalization to Al is widely used as a “proxy” of the clay content, generally  
626 representative of the finest and more efficient fraction for element sorption. The reference  
627 ( $[\text{Element}]/[\text{X}]$ ) represents the local background determined as the concentration ratio considered  
628 as free of anthropogenic influence.

629 Three heavy metal profile groups were identified in the sediment samples analyzed of the  
630 BH core. Group I includes Li (Figure 4), V, and Cd (Figure S4A); group II includes Ni (Figure 4)  
631 and Cr (Figure S4B); and group III includes Hg (Figure 4), Ag, Co, Cu, Mn, Pb, and Zn (Figure  
632 S4C). Elements of the first group were closely related to Al concentrations and the dynamics of the  
633 normalized concentrations were constant with mean  $\pm$  SD values of  $12.9 \pm 0.8 \text{ mg kg}^{-1}$  for Li,  $19.8$   
634  $\pm 1.0 \text{ mg kg}^{-1}$  for V, and  $0.046 \pm 0.007 \text{ mg kg}^{-1}$  for Cd (Figure 4, Figure S4A). The elements of the  
635 second group, Cr and Ni, had constant normalized concentrations along the core with values of  $13.9$   
636  $\pm 0.6 \text{ mg kg}^{-1}$  and  $4.8 \pm 0.2 \text{ mg kg}^{-1}$ , respectively. There were two peaks of normalized  
637 concentrations in the years  $1947 \pm 11$  and  $1913 \pm 16$  with an increase in concentrations up to 50%  
638 ( $20.4 \text{ mg kg}^{-1}$  for Cr (Figure S4B) and  $9.8 \text{ mg kg}^{-1}$  for Ni, Figure 4). Elements of the third group  
639 had increasing normalized concentrations from  $1958 \pm 9$  to more recent times (surface layers)  
640 (Figure 4, Figure S4C).

641 The natural background was established using the lowest element/Al concentration ratios in  
642 the core (38–39 cm depth). The relative enrichment factor (EF) of trace metals was used as an index  
643 to estimate the degree of anthropogenic contamination:

644 Equation 1:  $EF = ([\text{Element}]_{\text{sample}}/[\text{X}]_{\text{sample}}) / ([\text{Element}]_{\text{reference}}/[\text{X}]_{\text{reference}})$ .

645 Many pollution classes have been defined for EF values. Considering the low variability of the local  
646 background and following previous class, we assumed: EF values < 1.5 representing no or minimal  
647 anthropogenic enrichment; values between 1.5 and 3 representing a moderate anthropogenic  
648 signature; values between 3 and 10 indicating a moderately severe anthropogenic contribution; and  
649 values >10 underlining a severe anthropogenic impact. Every trace metal element measured in the  
650 core before  $1902 \pm 17$  had an EF < 1.5, representing minimal anthropogenic enrichment, except for  
651 Hg, which showed a higher EF (1.7). The two concentration peaks observed at  $1947 \pm 11$  for Cr  
652 and Ni (Figure 4, Figure S4B) correspond to a significant anthropogenic impact (EF = 2.0 for Ni).  
653 After  $1947 \pm 11$ , the pattern of normalized concentrations and associated EF remained low for some  
654 elements. The EF was mainly between 0.9 and 1.5; the relatively low concentrations of Li, V, Co,  
655 and Cd over the whole profile demonstrated that these elements are mainly from a lithogenic origin  
656 and that there was no significant anthropogenic source for these elements. The EF and  
657 concentrations of others trace metals (Ag, Cu, Hg, Pb, and Zn) progressively increased over time,  
658 with maximum EF values between 1.9 and 9.5. These values demonstrated a moderate to severe  
659 anthropogenic contamination in the order  $Zn < Pb < Ag < Cu < Hg$ .

660 Given that ordinary chemical reactions will not cause variations in the isotopic composition  
661 of Pb, it has been demonstrated that Pb is a powerful tracer of sources. To assess the origin of Pb  
662 in the sediment of the BH core, we used isotopic compositions as pertinent tools (Figure 4, Figure  
663 S4D, Figure S4E). Normalized Pb concentrations in the sediment core showed constant values ( $3.4$   
664  $\pm 0.1$  mg kg<sup>-1</sup>) from 40.5 to 18.5 cm depth (Figure S4D) with constant  $^{206}\text{Pb}/^{207}\text{Pb}$  ( $0.483 \pm 0.001$ )  
665 (Figure 4, Figure S4D) and  $^{206}\text{Pb}/^{208}\text{Pb}$  ( $1.198 \pm 0.002$ ) ratios (Figure S4D). Those ratios could be  
666 considered as the natural local background ratios, which is consistent with natural Pb isotope  
667 signatures referred to in previous studies performed in France coastal areas ( $^{206}\text{Pb}/^{207}\text{Pb}$  natural =  
668 1.195). At  $1924 \pm 14$ , a light peak of normalized Pb concentrations is observed correlated with a  
669 slight decrease of  $^{206}\text{Pb}/^{208}\text{Pb}$  ratio ( $1.190 \pm 0.002$ ) (Figure S4D). At  $1936 \pm 12$ , a light peak of

670  $^{206}\text{Pb}/^{207}\text{Pb}$  corresponded to the World War II period (Figure 4). Across more recent times,  
671  $^{206}\text{Pb}/^{207}\text{Pb}$  and  $^{206}\text{Pb}/^{208}\text{Pb}$  reached a natural local background ratio and normalized Pb  
672 concentrations increased more than threefold (Figure S4D). Concomitant variations in Pb  
673 concentrations and isotopes ratios showed the importance of anthropogenic activities and inputs in  
674 the Pb environmental cycle (Figure S4E).

675 The solvents (n-hexane, n-pentane, acetone, and iso-octane) used for Polychlorinated  
676 biphenyl (PCB) analyses were of trace analysis grade and supplied by SDS (France). PCB analyses  
677 were performed as described by Horri et al.<sup>68,69</sup>. Briefly, PCBs were analyzed by pressurized liquid  
678 extraction with the SpeedExtractor E-914 (Buchi Lab., Switzerland). The sulfur co-extracted with  
679 the organic compounds was removed using a tetrabutylammonium sulfite treatment before  
680 sequential purification with concentrated sulfuric acid and by adsorption chromatography on a  
681 Florisil column. The purified extracts were analyzed using gas chromatography with electron  
682 capture detection (GC- $\mu$ ECD, Agilent 7890B) equipped with two injectors, two columns (CP-Sil  
683 19 and HT08, Chrompack), and two electron capture detectors ( $\mu$ ECD Ni63). Among PCBs, the  
684 seven indicator PCB congeners were measured (CB28, 52, 101, 118, 138, 153, and 180), their sum  
685 being given as  $\Sigma$ 7PCBs. A few other congeners were also analyzed to describe a larger range of  
686 chlorination from 3 to 8 chlorine molecules (CB31, 44, 49, 105, 110, 128, 132, 149, 156, 170, 187,  
687 and 194) to check the appropriate resolution of the gas chromatography system, and because they  
688 can highlight underlying mechanisms acting on the distribution of organic contaminants. Analytical  
689 blanks were systematically measured every six samples. The blanks were about 0.2 pg  $\mu\text{l}^{-1}$ ,  
690 twentyfold less than the concentrations of the lowest standard of CB153 (i.e., < 0.1 ng  $\text{g}^{-1}$ ), and  
691 much less for other determinants. Finally, six replicates of a reference material (BCR-SRM1491b)  
692 were analyzed to determine the accuracy and precision of the method. PCB recoveries varied  
693 between 77% and 115%. Hydrophobic and persistent organic contaminants such as PCBs have a  
694 particular affinity for the organic material and differences in the sediment organic fraction can lead

695 to differences in contamination levels. Therefore, to overcome these differences and to compare the  
696 different fractions, a standardization procedure was applied and the PCB concentrations were  
697 expressed per g of organic carbon in dry sediment<sup>68</sup>.

### 698

### 699 **Historical archive documentation**

700 The departmental archives of Brest were consulted to find data, video, and pictures about the  
701 anthropic activities and events that occurred in the Bay of Brest that could have caused any pollution  
702 in the harbor area. In particular the, documents were analyzed concerning WWII (Figure S1C) and  
703 the Ocean Liberty vessel explosion. Some qualitative (videos, pictures) and quantitative (number  
704 of bombs per year, contents of the Ocean Liberty vessel) data were considered for the interpretation  
705 of shifts of the paleocommunities.

### 706

### 707 **Quantification and Statistical Analysis**

708  $\alpha$  (intraspecific) and  $\beta$  (interspecific) diversity and the diversity index were calculated using the  
709 vegan R packages Dplyr and TidyR of R v3.4.4<sup>70</sup>.  $\alpha$  diversity analyses were used to discriminate  
710 observed richness patterns in the BH core for all *seDNA* extraction methods (TOT, IN, and EX)  
711 Table S3). A non-metric multi-dimensional (NMDS) analysis inferred from a dissimilarity matrix  
712 based on the Jaccard index was carried out to analyze  $\beta$  diversity among TOT, IN, and EX samples  
713 of the BH core (Figure S2D). After the NMDS analysis, the ANOSIM test was performed to identify  
714 statistically similar groups of samples. Plots were created using the ggplot2 R package<sup>71</sup>.

715 A chronological clustering of the BH, DE, and EE samples was performed to detect the  
716 dates and the hierarchical order of modification in the ASV paleocommunity structure. Prior to this  
717 analysis, relative abundances of ASV taxonomically assigned to the same genera/groups were  
718 cumulated. This cumulated ASV was named with the genus and/or taxonomic groups to which it  
719 belongs (according to PR<sup>2</sup> annotation). ASV not assigned to any species or genera assigned were

720 cumulated in a group named Unknown. For simplicity, in the Results section the taxonomic name  
721 of the genus or groups is used to indicate the cumulated ASVs. Separate MRT analyses<sup>72</sup> were  
722 performed on the protist, dinoflagellate, and stramenopile cumulated ASV data from the BH, DE,  
723 and EE samples. This time-constrained analysis was performed according to the instructions  
724 proposed by Bocard et al.<sup>73</sup>, and the size of each tree was selected using the graphs of the relative  
725 error. The R package mvpart was used for this analysis. MRT level 1 is shown in Figure 2, Figure  
726 3, and Figure S3.

727

## 728 **Supplementary information**

729 **Data S1. Dating of Elorn Estuary (EE), Daoulas Estuary (DE), and Brest Harbor (BH) cores**

730 **Related to STAR Methods.. A)** Elorn Estuary (EE) sediment chronology. **B)** Daoulas Estuary  
731 (DE) sediment chronology. **C)** Brest Harbor (BH) sediment chronology.

732

733 **Data S2. Taxa known to form resting stages for the. Related to STAR Methods. A)** V7 barcode.

734 **B)** V4 barcode.

735

736 **Video S1. Core sampling, *in situ* and lab work on sediment cores. Related to STAR Methods.**

737

## 738 **References**

739 1. Tett, P., Gowen, R.J., Painting, S.J., Elliott, M., Forster, R., Mills, D.K, Bresnan, E.,  
740 Capuzzo, E., Fernandes, T.F., Foden, J., Geider, R.J., Gilpin, L. C., Huxham, M.,  
741 McQuatters-Gollop, A.L, Malcolm, S.J., Saux-Picart, S., Platt, T., Racault, M.-F.,  
742 Sathyendranath, S., van der Molen, J., and Wilkinson, M. (2013). Framework for  
743 understanding marine ecosystem health. *Mar. Ecol. Prog. Ser.* 494, 1–27.

- 744 2. Waters, C.N., Zalasiewicz, J., Summerhayes, C., Barnosky, A.D., Poirier, C., Galuszka,  
745 A., Cearretz, A., Edgeworth, M., Ellis, E.C., Ellis, M., Jeandel, C., Leinfelder R., McNeill,  
746 J.R., deB Richter, R., Steffen, W., Vidas, D., Wagreich, M., Williams, M., Zhisheng, A.,  
747 Grinevald, J., Odada, E., Oreskes, N., and Wolfe, A.P. (2016). The Anthropocene is  
748 functionally and stratigraphically distinct from the Holocene. *Science* 351 aad2622.
- 749 3. Jonkers, L., Hillebrand, H., and Kucera, M. (2019). Global change drives modern plankton  
750 communities away from the pre-industrial state. *Nature* 570, 372–375.
- 751 4. Fordham, D.A., Jackson, S.T., Brown, S.C., Huntley, B., Brook, B.W., Dahl-Jensen, D.,  
752 Gilbert, M.T.P., Otto-Bliesner, B.L., Svensson, A., Theodoridis, S., Wilmshurst, J.M.,  
753 Buettel, J.C., Canteri, E., McDowell, M., Orlando, L., Pilowsky, J., Rahbek, C., and  
754 Nogues-Bravo, D. (2020). Using paleo-archives to safeguard biodiversity under climate  
755 change. *Science* 369, eabc5654.
- 756 5. Boere, A.C., Sinninghe Damsté, J.S., Rijpstra, W.I.C., Volkman, J. K., and Coolen, M.J.L.  
757 (2011). Source-specific variability in post-depositional DNA preservation with potential  
758 implications for DNA based paleoecological records. *Org. Geochem.* 42, 1216–1225.
- 759 6. Coolen, M.J.L (2011) 7000 years of *Emiliana huxleyi* viruses in the Black Sea. *Science*  
760 333, 451–452.
- 761 7. Klouch, K.Z., Schmidt, S., Andrieux-Loyer, F., Le Gac, M., Hervio-Heath, D., Qui-Minet,  
762 Z.N., Quéré, J., Bigeard, E., Guillou, L., and Siano, R. (2016). Historical records from dated  
763 sediment cores unveiled the multidecadal dynamics of the toxic dinoflagellate *Alexandrium*  
764 *minutum* in the Bay of Brest (France). *FEMS Microbiol. Ecol.* 92, fiw101
- 765 8. Konkell, R., Toruńska-Sitarz, A., Cegłowska, M., Ežerinskis, Ž. Šapolaitė, J., Mažeika, J.,  
766 and Mazur-Marzec, H. (2020). Blooms of toxic cyanobacterium *Nodularia spumigena* in  
767 Norwegian fjords during Holocene warm periods. *Toxins* 12, 257.

- 768 9. Stoof-Leichsenring, K.R., Epp, L.S., Trauth, M.H., and Tiedemann, R. (2012). Hidden  
769 diversity in diatoms of Kenyan Lake Naivasha: a genetic approach detects temporal  
770 variation. *Mol. Ecol.* *21*, 1918–1930.
- 771 10. Coolen, M.J.L., Orsi, W.D., Balkema, C., Quince, C., Harris, K., Sylva, S.P., Filipova-  
772 Marinova, M., and Giosan, L. (2013). Evolution of the plankton paleome in the Black Sea  
773 from the Deglacial to Anthropocene. *PNAS* *110*, 8609–8614.
- 774 11. Lejzerowicz, F., Voltsky, I, and Pawlowski, J. (2013). Identifying active foraminifera in the  
775 Sea of Japan using metatranscriptomic approach. *Deep Sea Res. Part II: Topical Studies in*  
776 *Oceanograph* *86–87*, 214–220.
- 777 12. Hou, W., Dong, H., Li, G., Yang, J., Coolen, M.J.L., Liu, X., Wang, S., Jiang, H., Wu, X.,  
778 Lian., B., and Wan, Y. (2014). Identification of photosynthetic plankton communities using  
779 sedimentary ancient DNA and their response to late-Holocene climate change on the  
780 Tibetan Plateau. *Sci. Rep.* *4*, 6648.
- 781 13. Capo, E. Debroas, D., Arnaud, F., Guillemot, T., Bichet, V., Millet, L., Gauthier, E., Massa,  
782 C., Develle, A.-L., Pignol, C., Lejzerowicz, F., and Domaizon, I. (2016). Long-term  
783 dynamics in microbial eukaryotes communities: a palaeolimnological view based on  
784 sedimentary DNA. *Mol. Ecol.* *25*, 5925–5943.
- 785 14. Giosan, L., Orsi, W.D., 2,3, Coolen, M.J.L., Wuchter, C. Dunlea, A.G., Thirumalai, K.,  
786 Munoz, S.E., Clift, P.D., Donnelly, J.P., Galy, V., and Fuller, D.Q. (2018). Neoglacial  
787 climate anomalies and the Harappan metamorphosis. *Clim. Past* *14*, 1669–1686.
- 788 15. More, K.D., Orsi, W.D., Galy, V., Giosan, L., He, L., Grice, K., and Coolen, M.J.L. (2018).  
789 A 43 kyr record of protist communities and their response to oxygen minimum zone  
790 variability in the Northeastern Arabian Sea. *Earth Planet. Sci. Lett* *496*, 248–256.

- 791 16. De Schepper, S., Ray, J.R., Sandnes Skaar, K., Sadatzki, H., Ijaz, U, Z., Stein, R., and  
792 Larsen, A. (2019). The potential of sedimentary ancient DNA for reconstructing past sea  
793 ice evolution. *ISME J.* *13*, 25566–2577.
- 794 17. Capo, E., Rydberg, Tolu, J., Domaizon, I., Debroas, D., Bindler R., and Bigler, C. (2019).  
795 How does environmental inter-annual variability shape aquatic microbial communities? A  
796 40-year annual record of sedimentary DNA from a boreal lake (Nylandssjön, Sweden).  
797 *Front. Ecol. Evol.* *7*, 245.
- 798 18. Keck, E., Millet, L., Debroas, D., Etienne, D., Galop, D., Rius, D., and Domaizon I. (2020).  
799 Assessing the response of micro-eukaryotic diversity to the Great Acceleration using lake  
800 sedimentary DNA. *Nature Comm.* *11*, 3831.
- 801 19. Pomeroy, L. R. (1974). The ocean's food web, a changing paradigm. *BioScience* *24*, 499–  
802 504.
- 803 20. Azam, F., Fenchel, T., Field, J.G., Gray, J.S., Meyer-Reil, L.A., and Thingstad, F. (1983).  
804 The ecological role of water-column microbes in the Sea. *MEPS* *10*, 257–263.
- 805 21. Worden, A.Z., Follows, M.J., Giovannoni, S.J., Zimmermann, A.E., and Keeling, P.J. (2015)  
806 Rethinking the marine carbon cycle: Factoring in the multifarious lifestyles of microbes.  
807 *Science* *347*, 1257594
- 808 22. Armbrrecht, L.H., Coolen, M.J.L., Lejzerowicz, F., George, S.C., Negandhi, K., Suzuki, Y.,  
809 Young, J., Foster, N.R., Armand, L.K., Cooper, A., Ostrowski, M., Focardi, A., Stat, M.,  
810 Moreau, J.W., and Weyrich, L.S. (2019). Ancient DNA from marine sediments: Precautions  
811 and considerations for seafloor coring, sample handling and data generation. *Earth Sci. Rev.*  
812 *196*, 102887.
- 813 23. Taberlet, P., Coissac, E., Hajibabaei, M., and Rieseberg, L.H. (2012). Environmental DNA.  
814 *Mol. Ecol.* *21*, 1789–1793.

815 24. Zinger, L., Chave, J., Coissac, E., Iribar, A., Louisanna, E., Manzi, S., Schilling, V.,  
816 Schimann, H., Sommeria-Klein, G., and Taberlet, P. (2016). Extracellular DNA extraction  
817 is a fast, cheap and reliable alternative for multi-taxa surveys based on soil DNA. *Soil. Biol.*  
818 *Biochem.* *96*, 16–19.

819 25. Leander, B.S., Lloyd, S.A.J., Marshall, W., and Landers, S.C. (2006). Phylogeny of Marine  
820 Gregarines (Apicomplexa) — *Pterospora*, *Lithocystis* and *Lankesteria* — and the Origin(s)  
821 of Coelomic Parasitism. *Protist* *157*, 45–60.

822 26. de Vargas, C., Audic, S., Henry, N., Decelle, J., Mahé, F., Logares, R., Lara, E., Berney, C.,  
823 Le Bescot, N., Probert, I., Carmichael, M., Poulain, J., Romac, S., Colin, S., Aury, J.M.,  
824 Bittner, L., Chaffron, S., Dunthorn, M., Engelen, S., Flegontova, O., Guidi, L., Horak, A.,  
825 Jaillon, O., Lukes, J., Malviya, S., Morard, R., Mulot, M., Scalco, E., Siano, R., Vincent, F.,  
826 Zingone, A., Dimier, C., Picheral, M., Searson, S., Kandels-Lewis, S., Acinas, S. G., Bork,  
827 P., Bowler, C., Gorsky, G., Grimsley, N., Hingamp, P., Iudicone, D., Not, F., Ogata, H.,  
828 Pesant, S., Raes, J., Sieracki, M., Speich, S., Stemman, L., Sunagawa, S., Weissenbach, J.,  
829 Wincker, P., Karsenti, E., and Tara Oceans Expedition, Tara Oceans Coordinators (2015).  
830 Eukaryotic plankton diversity in the sunlit global ocean. *Science* *348*, 1–12

831 27. Ramond, P., Sourisseau, M., Simon, N., Sarah, R., Schmitt, S., Rigaut-Jalabert, F., Henry,  
832 N., de Vargas, C., and Siano, R. (2019). Coupling between taxonomic and functional  
833 diversity in protistan coastal communities. *Environ. Microbiol.* *21*, 730–749.

834 28. Forster, D., Dunthorn, M., Mahé, F., Dolan, J., Audic, S., Bass, D., Bittner, L., Boutte, C.,  
835 Christen, R., Claverie, J.-M., Decelle, J., Edvardsen, B., Egge, E., Eikrem, W., Gobet, A.,  
836 Kooistra, W.H.C.F., Logares, R., Massana, R., Montresor, M., Not, F., Ogata, O.,  
837 Pawlowski, J., Pernice, M., Romac, S., Shalchian-Tabrizi, K., Simon, N., Richards, T.,  
838 Santini, S., Sarno, D., Siano, R., Vaultot, D., Wincker, P., Zingone, A., de Vargas, C., and

- 839 Stoeck, T. (2016). Benthic protists: the under-charted majority. *FEMS Microbiol. Ecol.* *92*,  
840 fiw120.
- 841 29. del Campo, J., Heger, T., Rodriguez-Martinez, R., Worden, A.Z., Richards, T.A., Massana,  
842 R., and Keeling, P.J. (2019). Assessing the diversity and distribution of apicomplexans in  
843 host and free-living environments using high-throughput amplicon data and a  
844 phylogenetically informed reference framework. *Front. Microbiol.* *10*, 2373.
- 845 30. Mahé, F., de Vargas, C., Bass, D., Lucas, C., Stamatakis, A., Lara, E., Singer, D., Mayor,  
846 D., Bunge, J., Sernaker, S., Siemensmeyer, T., Trautmann, I., Romac, S., Berney, C.,  
847 Kozlov, A., Mitchell, E.A.D., Seppey, C.V.W., Egge, E., Lentendu, G., Wirth, R., Trueba,  
848 G, and Dunthorn, M. (2017). Parasites dominate hyperdiverse soil protist communities in  
849 Neotropical rainforests. *Nat. Ecol. Evol.* *1*, 0091.
- 850 31. Massana, R., del Campo, J., Sieracki, M. E., Audic, S., and Logares, R. (2014). Exploring  
851 the uncultured microeukaryote majority in the oceans: reevaluation of ribogroups within  
852 stramenopiles. *ISME J.* *8*, 854–866.
- 853 32. Ashwood, T.L., and Olsen, C.R. (1988). Pearl Harbour bombing attack: a contamination  
854 legacy revealed in the sedimentary record. *Mar. Pollut. Bull.* *19*, 68–71.
- 855 33. Dendievel, A.-M., Mourier, B., Coynel, A., Evrard, O., Labadie, P., Ayrault, S., Debret, M.,  
856 F. Koltalo, Copard, Y., Faivre, Q., Gardes, T., Vauclin, S., Budzinski, H., Grosbois, C.,  
857 Winiarski, T., and Desmet, M. (2020). Spatio-temporal assessment of the polychlorinated  
858 biphenyl (PCB) sediment contamination in four major French river corridors (1945–2018),  
859 *Earth Syst. Sci. Data* *12*, 1153–1170.
- 860 34. Castro-Jiménez, J., Deviller, G., Ghiani, M., Loos, R., Mariani, G., Skejo, H., Umlauf, G.,  
861 Wollgast, J., Laugier, T., Héar-Moisan, K., Léauté, F., Munsch, C., Tixier, C., and  
862 Tronczyński, J., (2008). PCDD/F and PCB multi-media ambient concentrations, congener

863 patterns and occurrence in a Mediterranean coastal lagoon (Etang de Thau, France).  
864 *Environ. Pollut.* *156*, 123–135.

865 35. Elsenreth, S., Capel, P.D., Robbins, J.A., and Bourbonniere, R. (1989). Accumulation and  
866 diagenesis of chlorinated hydrocarbons in lacustrine sediments. *Environ. Sci. Technol.* *23*,  
867 1116–1126.

868 36. Schneider, A. R., Stapleton, H. M., and Baker, J. E. (2001) Recent declines in PAH, PCB,  
869 and toxaphene levels in the northern great lakes as determined from high resolution  
870 sediment cores. *Environ. Sci. Technol.* *35*, 3809–3815.

871 37. Lambert, C., Penaud, A., Vidal, M., Klouch, K.Z., Gregoire, G., Ehrhold, A., Eynaud, F.,  
872 Schmidt, S., Ragueneau, O., and Siano R. (2018). Human-induced river runoff overlapping  
873 natural climate variability over the last 150 years: Palynological evidence (Bay of Brest,  
874 NW France). *Glob. Planet. Change* *160*, 109–122.

875 38. Batten, S.D., and Burkill, P.H. (2010). The Continuous Plankton Recorder: Towards a  
876 global perspective. *J. Plankton. Res.* *32*, 1619–1621

877 39. Quéguiner, B., and Tréguer, P. Studies on the phytoplankton in the Bay of Brest (Western  
878 Europe). (1984). Seasonal variations in composition biomass and production in relation to  
879 hydrological and chemical features (1981–1982). *Bot. Mar.* *27*, 449–459.

880 40. Del Amo, Y., Le Pape, O., Tréguer, P., Quéguiner, B., Menesguen, A., and Aminot, A.  
881 (1997). Impacts of high-nitrate freshwater inputs on macrotidal ecosystems. I. Seasonal  
882 evolution of nutrient limitation for the diatom-dominated phytoplankton of the Bay of Brest  
883 (France). *Mar. Ecol. Prog. Ser.* *161*, 213–224.

884 41. Boyce, D.G., Lewis M.R., and Worm, B. (2010). Global phytoplankton decline over the  
885 past century. *Nature* *466*, 591–596.

886 42. Burrows, M.T., Bates, A.E., Costello, M.J., Edwards, M., Edgar, G.J., Fox, C.J., Halpern,  
887 B.S., Hiddink, J.G., Plinsky, M.L., Batt, R.D., Molinos, J.G., Payne, B.L., Schoeman, D.S.,

- 888 Stuart-Smith, R.D., and Poloczanska, E.S. (2019). Ocean community warming responses  
889 explained by thermal affinities and temperature gradients. *Nat. Clim. Change* 9, 959–963.
- 890 43. Liu, D., Shen, X., Di, B., Shi, Y., Keesing, J., and Wang, Y. (2013). Palaeoecological  
891 analysis of phytoplankton regime shifts in response to coastal eutrophication. *Mar. Ecol.*  
892 *Prog. Ser.* 475, 1–14
- 893 44. Ibrahim, A., Capo, E., Wessels, M., Martin, I., Meyer, D., Schleheck, D., and Epp, L.S.  
894 (2020) Anthropogenic impact on the historical phytoplankton community of Lake  
895 Constance reconstructed by multimarker analysis of sediment-core environmental DNA.  
896 *Mol. Ecol.* <https://doi.org/10.1111/mec.15696>
- 897 45. Capo, E. Domaizon, I., Maier, D., Debroas, D., and Bigler, C. (2017). To what extent is the  
898 DNA of microbial eukaryotes modified during burying into lake sediments? A repeat-coring  
899 approach on annually laminated sediments. *J. Paleolim.* 58, 479–495.
- 900 46. Cao, X., Xu, X., Bian, R., Wang, Y., Yu, H., Xu Y., Duan, G., Bi, L., Chen, P., Gao, S.,  
901 Wang, J., Peng, J., and Qu, J. (2020). Sedimentary ancient DNA metabarcoding delineates  
902 the contrastingly temporal change of lake cyanobacterial communities. *Water Res.* doi:  
903 10.1016/j.watres.2020.116077.
- 904 47. Bálint, M., Pfenninger, M., Grossart, H.-P., Taberlet, P., Vellend, M., Leibold, M.A.,  
905 Englund, G., and Bowler D. (2018). Environmental DNA time series in ecology. *Trends*  
906 *Ecol. Evol.* 12. 945–957.
- 907 48. Monchamp, M.-E., Enache, J., Turko, P., Pomati, F., Rîșnoveanu, G., and Spaak, P. (2017).  
908 Sedimentary and egg-bank DNA from 3 European lakes reveal concurrent changes in the  
909 composition and diversity of cyanobacterial and *Daphnia* communities. *Hydrobiologia* 88,  
910 155–172.

- 911 49. Pal, S., Gregory-Eaves, I., and Pick, F.R. (2015). Temporal trends in cyanobacteria revealed  
912 through DNA and pigment analyses of temperate lake sediment cores. *J. Paleolimnol.* 54,  
913 87–101.
- 914 50. Pawlowski, J., Kelly-Qui, M., Altermatt, F., Apothéloz-Perret-Gentil, L., Beja, P., Boggero,  
915 A., Borja, A., Bouchez, A., Cordier, T., Domaizon, I., Feio, M.J., Filipe, A.F., Fornaroli, R.,  
916 Graf, W., Herder, J., van der Hoorn, B., Jones, I., Sagova-Mareckova, M., Moritz., C.,  
917 Barquín, J., Piggott, J.J., Pinna, M., Rimet, F., Rinkevich, B., Sousa-Santos, C., Specchia,  
918 V., Trobajo, R., Vasselon, V., Vitecek, S., Zimmerman, J., Weigand, A., Leese, F., and  
919 Kahlert, M., (2018). The future of biotic indices in the ecogenomic era: Integrating (e)DNA  
920 metabarcoding in biological assessment of aquatic ecosystems. *Sci. Total Environ.* 637–  
921 638, 1295–1310.
- 922 51. Coclet, C., Garnier, C., Delphy, F., Jamet, D., Durrieu, G., Le Poupon, C., Mayer, and M.,  
923 Misson, B. (2018). Trace metal contamination as a toxic and structuring factor impacting  
924 ultraphytoplankton communities in a multicontaminated Mediterranean coastal area. *Prog.*  
925 *Oceanogr.* 163, 196–213.
- 926 52. Jia, J., Gao, Y., Lu., Y., Shi, K., Li, Z., and Wang, S. (2020). Trace metal effects on gross  
927 primary productivity and its associative environmental risk assessment in a subtropical lake,  
928 China. *Environ. Pollut.* 259, 113848.
- 929 53. Kleppel, G.S., and McLaughlin, J.J.A. (1980). PCB toxicity to phytoplankton: effects of  
930 dose and density-dependent recovery responses. *Bull. Environm. Contam. Toxicol.* 24, 696–  
931 703.
- 932 54. Herzi, F., Jean, N., Hlaili, A.S., and Mounier, S. (2014). Three-dimensional (3-D)  
933 fluorescence spectroscopy analysis of the fluorescent dissolved organic matter released by  
934 the marine toxic dinoflagellate *Alexandrium catenella* exposed to metal stress by zinc or  
935 lead. *J. Phycol.* 50, 665–674

- 936 55. Bausch, A.R., Boatta, F., Morton, P.L., McKee, K.T., Anderson, R.F., Gomes, H.R., and  
937 Goes, J.I. (2017). Elevated toxic effect of sediments on growth of the harmful dinoflagellate  
938 *Cochlodinium polykrikoides* under high CO<sub>2</sub>. *Aquat. Microb. Ecol.* 80, 139–152.
- 939 56. Ragueneau, O., Chauvaud, L., Leynaert, A., Thouzeau, G., Paulet, Y.M., Bonnet., Lorrain  
940 A, Grall, J., Corvaisier, R., Le Hir, M., Jean, F., and Clavier, J. (2002). Direct evidence of  
941 a biologically active coastal silicate pump: Ecological implications. *Limnol. Oceanog.* 47,  
942 1849–1854.
- 943 57. Guillaud, J.-F., and Bouriel, L. (2007). Relation concentration-débit et évolution temporelle  
944 du nitrate dans 25 rivières de la région Bretagne (France). *Revue Des Sciences de L'eau*,  
945 20, 213.
- 946 58. Trommer, G., Leynaert, A., Klein, C., Naegelen, A., and Beker, B. (2013). Phytoplankton  
947 phosphorus limitation in a North Atlantic coastal ecosystem not predicted by nutrient load.  
948 *J. Plank. Res.* 35, 1207–1219.
- 949 59. Reimer, P.J., Bard, E., Bayliss, A., Beck, J.W., Blackwell, P.G., Ramsey, C.B., Buck, C.E.,  
950 Cheng, H., Edwards, R.L., Friedrich, M., Grootes, P.M., Guilderson, T.P., Hafliðason, H.,  
951 Hajdas, I., Hatté, H., Heaton, T.J., Hoffmann, D.L., Hogg, A.G., Hughen, K.A., Kaiser, K.  
952 F., Kromer, B., Manning, S.W., Niu, M., Reimer, R.W., Richards, D.A., Scott,  
953 E.M., Southon, J.R., Staff, R.A., Turney, C.S.M. and van der Plicht, J. (2013). IntCal13 and  
954 Marine13 radiocarbon age calibration curves 0–50,000 years cal BP. *Radiocarbon* 55, 1869–  
955 1887.
- 956 60. Gregoire, G., Le Roy, P., Ehrhold, A., Jouet, G., and Garlan, T. (2017). Control factors of  
957 Holocene sedimentary infilling in a semi-closed tidal estuarine-like system: the bay of Brest  
958 (France). *Mar. Geol.* 385, 84–100.
- 959 61. Kim, J.H., Kim, J.H., Wang, P., Park, B.S., and Han, M.S. (2016). An improved quantitative  
960 real-time PCR assay for the enumeration of *Heterosigma akashiwo* (Raphidophyceae) cysts

961 using a DNA debris removal method and a cyst-based standard curve. PLoS One 11,  
962 e0145712.

963 62. Gilbert, M.T. P., Bandelt, H.-J., Hofreiter, M., and Barnes, I. (2005). Assessing ancient  
964 DNA studies. Trends Ecol Evol 20, 541–544.

965 63. Martin, M. (2011). Cutadapt removes adapter sequences from high-throughput sequencing  
966 reads. EMBnet J 17, 10–12.

967 64. Callahan, B.J., McMurdie, P.J., Rosen, M.J., Han, A.W., Johnson, A.J.A., and Holmes, S.P.  
968 (2016). DADA2: high-resolution sample inference from Illumina amplicon data. Nat.  
969 Methods 13, 581–583.

970 65. Guillou, L., Bachar, D., Audic, S., Bass, D., Berney, C., Bittner, L., Boutte, C., Burgaud,  
971 G., de Vargas, C., Decelle, J., del Campo, J., Dolan, J.R., Dunthorn, M., Edvardsen, B.,  
972 Holzmann, M., Kooistra, W.H.C.F., Lara, E., Le Bescot, N., Logares, R., Mahé, F.,  
973 Massana, R., Montessor, M., Morard, R., Not, F., Pawlowski, J., Probert, I., Sauvadet, A.-  
974 L., Siano, R., Stoeck, T., Vaultot, D., Zimmermann, P., and Christen, R. (2013). The protist  
975 Ribosomal reference database (PR<sup>2</sup>): a catalog of unicellular eukaryote small subunit rRNA  
976 sequences with curated taxonomy. Nucleic Acids Res. 41, D597–D604.

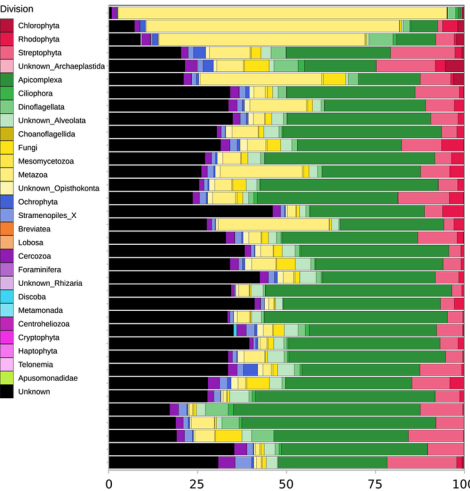
977 66. Okasenen, J., Kindt, R., Legendre, P., O’Hara, B., Simpson, G.L., Solymos, P., Henry, M.,  
978 Stevens, H., and Wagner, H. (2008). The vegan Package. <http://cran.r-project.org/>,  
979 <http://vegan.r-forge.r-project.org>.

980 67. McMurdie, P.J, and Holmes S (2013). phyloseq: An R package for reproducible interactive  
981 analysis and graphics of microbiome census Data. Plos One 8, e61217.

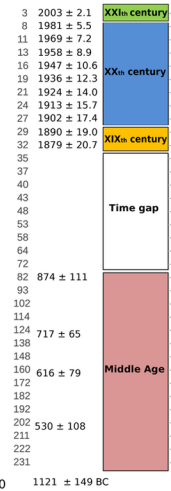
982 68. Horri, K., Alfonso, S., Cousin, X., Munsch, C., Loizeau, V., Aroua S., Bégout, M.-L., and  
983 Ernande, B. (2018). Fish life-history traits are affected after chronic dietary exposure to an  
984 environmentally realistic marine mixture of PCBs and PBDEs. Sci. Tot. Environ. 610–611,  
985 531–545

- 986 69. Breivik, K., Sweetman, A., Pacyna, J.M., and Jones, K.C. (2002). Towards a global  
987 historical emission inventory for selected PCB congeners — a mass balance approach: 2.  
988 Emissions. *Sci. Tot. Environ.* 290, 199–224.
- 989 70. R Core Team R: A Language and Environment for Statistical Computing. R Foundation for  
990 Statistical Computing, Vienna. <https://www.R-project.org> (2018).
- 991 71. Wickham, H. (2009). *Ggplot2. Elegant Graphics for data analysys* (Springer International  
992 Publishing).
- 993 72. De'ath, G. (2002) Multivariate regression trees: a new technique: a new technique for  
994 modeling species - environment relationships. *Ecology* 83, 1105–1117.
- 995 73. Borcard, D., Gillet, F., and Legendre, P. (2011) *Numerical Ecology with R.* (Springer, New  
996 York).
- 997

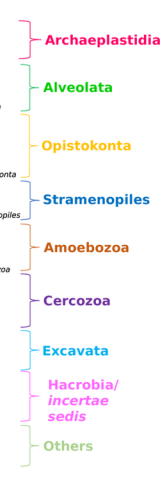
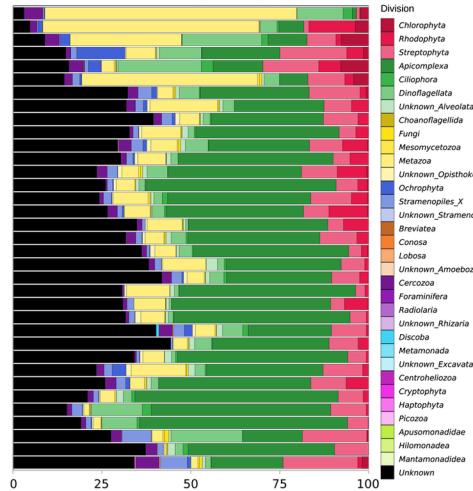
Barcode: V7 18S rDNA

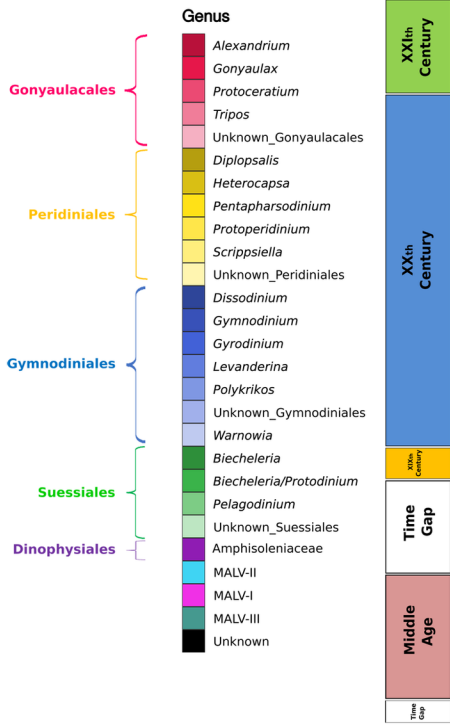


Depth (cm) Time period



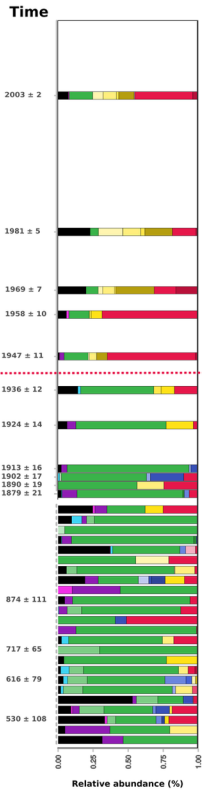
Barcode: V4 18S rDNA



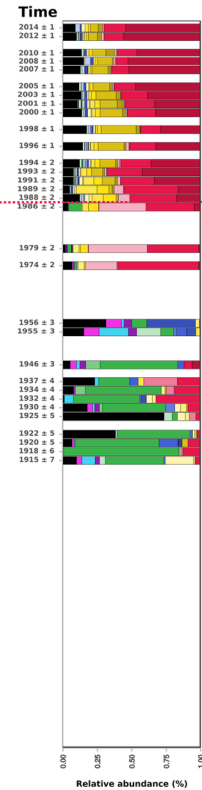


..... BREAK POINTS DETECTED IN THE COMMUNITY STRUCTURE (MRT ANALYSIS)

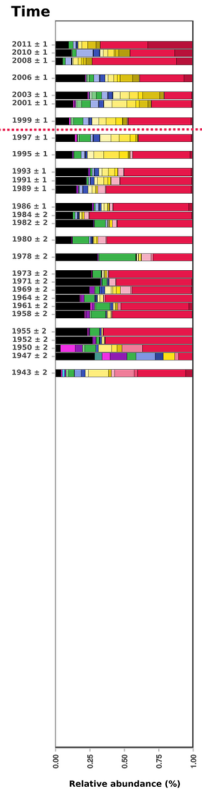
**Brest Harbour (BH)**

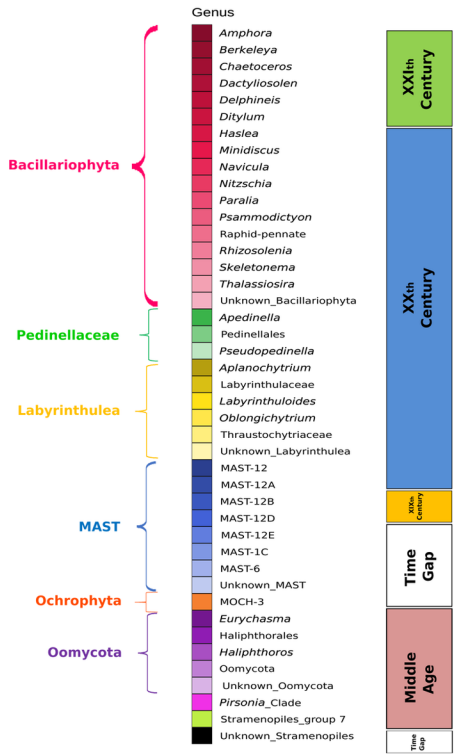


**Daoulas Estuary (DE)**



**Elorn Estuary (EE)**





Bacillariophyta

Pedinellaceae

Labyrinthulea

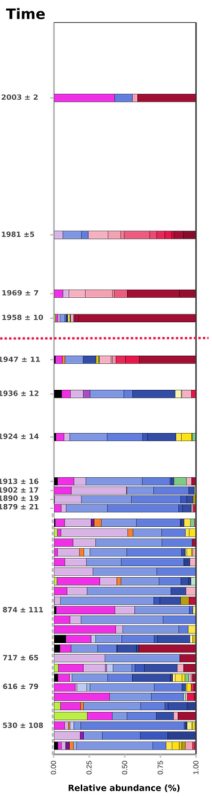
MAST

Ochrophyta

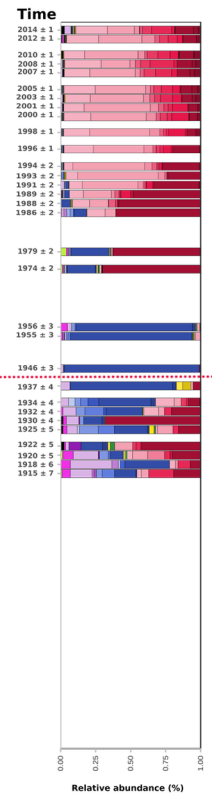
Oomycota

..... BREAK POINTS DETECTED IN THE COMMUNITY STRUCTURE (MRT ANALYSIS)

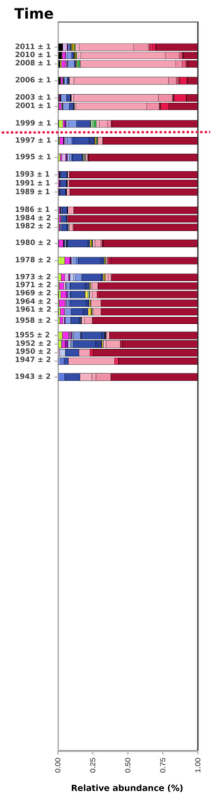
**Brest Harbour (BH)**



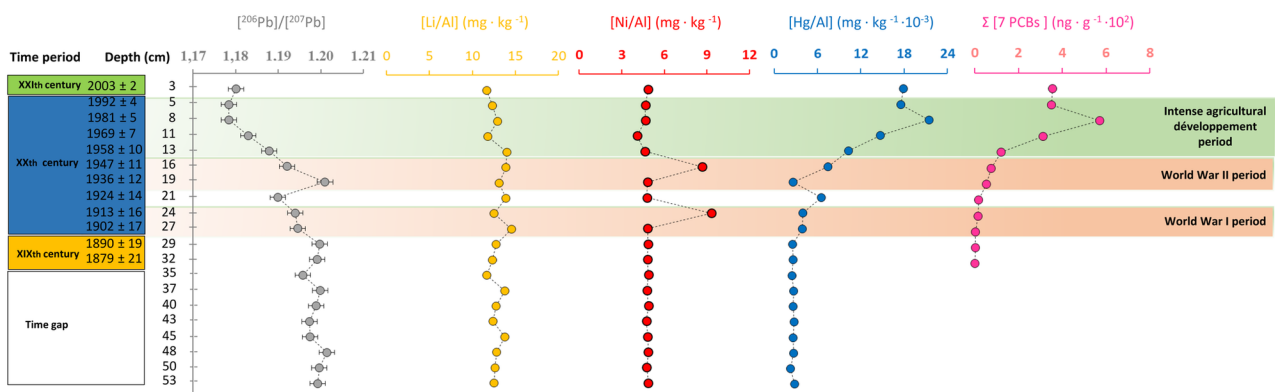
**Daoulas Estuary (DE)**



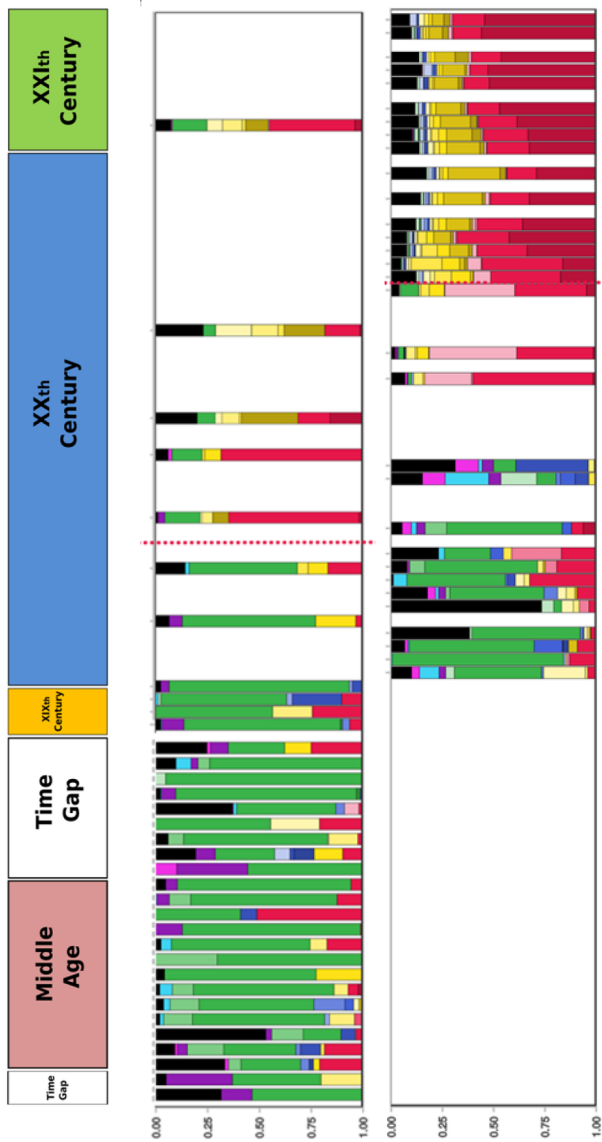
**Elorn Estuary (EE)**



1998

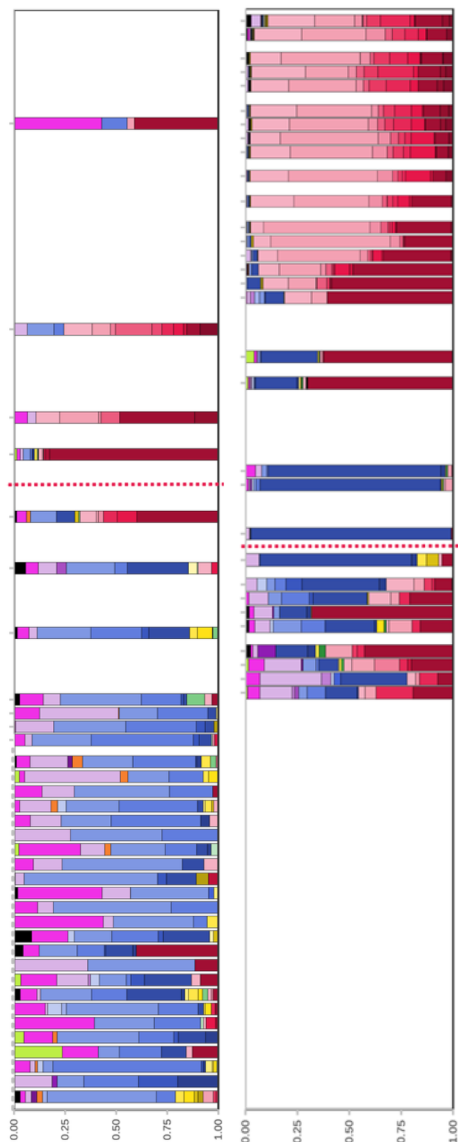


# Dinoflagellates



Suessiales → Gonyaulacales

# Stramenopiles



MARine Stramenopiles → Diatoms